Final Report

Turbulence Measurements on a Flap-Edge Model

NASA-Ames University Consortium
NCC2-5140
March 31, 1998

Patrick Moriarty+, Peter Bradshaw+, Brian Cantwell+, James Ross*
+Stanford University, *NASA Ames

Abstract

Turbulence measurements have been made on a flap-edge and leading-edge slat model using hot-wire anemometry, and, later, particle image velocimetry. The properties of hot-wire anemometry were studied using facilities at NASA Ames Research Center. Hot-film probes were used because of their durability, but cross-films were limited by non-linear end effects. As a warm-up exercise, hot-film probes were used to measure velocities in the farfield wake of a cylinder with an airfoil in the near-field wake. The airfoil reduced the drag coefficient of the system by 10%. A single-wire hot-film probe was used to measure velocity profiles over the top of a NACA 63_2-215 Mod. B wing with a Fowler flap and leading-edge slat. Results showed the size of slat wake was dependent upon the slat deflection angle. Velocity increased through the slat gap with increased deflection. The acoustically modified slat decreased the chance of separation. Measurements were taken at the flap edge with a single hot-film. Trends in the data indicate velocity and turbulence levels increase at the flap edge. The acoustically modified flap modifies the mean flow near the flap edge. Correlations were made between the hot-film signal and the unsteady pressure transducers on the wing which were published in a NASA CDTM. The principles of particle image velocimetry (PIV) were studied at Florida State University. Spectral PIV was used to measure the spectra of a subsonic jet. Measured frequencies were close to the predicted frequency of jet shedding. Spectral PIV will be used to measure the spectra of the slat flow in the second 7-x10-ft. wind tunnel test. PIV has an advantage that it can measure velocity and spectra of the entire flowfield instantaneously. However, problems arise when trying to store this massive amount of PIV data. Support for this research has continued through a NASA Graduate Student Program Fellowship which will end in June 1999. The thesis should be completed by this time.

Hot-wire

Most of the period before the first 7-x10-ft. wind tunnel test was spent learning about hot-wire anemometry. Due to a dusty climate in the wind tunnel, hot-film probes were considered more reliable than fragile hot-wires. These hot-films required a different anemometer system than used with standard hot-wires. The extra current needed by the hot-films required the use of DISA bridges instead of the Watmuff designed anemometers used in the Fluid Mechanics Laboratory.[1] The DISA bridges also gave a much higher frequency response (50 kHz at 100 m/s) than the Watmuff anemometers. In addition, the DISA anemometers allowed much longer cable lengths of 20m. This provided greater freedom of movement of the hot-films and placement of the anemometers on the outside of the test section.

Considerable effort was made to examine the ambient temperature dependence of the hot-film calibration. A study using a small calibration tunnel and a space heater was done by performing calibrations at different mean flow temperatures over a 26°C range.

Results from this study determined that a linear relation between temperature and the calibration coefficients was sufficient.

A study was performed to determine the most effective method of using a King's Law calibration. It was discovered that the slope, intercept and exponent were all functions of the velocity range. In order to approximate a true King's Law (i.e. velocity coefficient near 0.5), the lowest range of velocities (down to about 4 m/s) had to be included. The entire range of the calibration manometer was used to measure velocities from 4 m/s to 110 m/s. The velocity at some locations on the wing exceeded this maximum calibration velocity. Therefore, a higher pressure manometer will be used in future tests. Also, the speed and ease of the calibration process will be improved by the use of a pressure transducer instead of a liquid manometer.

During the wind tunnel test, calibrations were taken twice daily. Error measurements of these calibrations were taken at the end of the day. The maximum error in mean velocity occurred around 100 m/s and was approximately 5%. In order to reduce this error, it would be preferable to calibrate the hot-films in situ and over a higher velocity range. However, it would be impossible to perform an in situ calibration because of the time required to bring the 7-x10-ft. tunnel to a steady-state velocity condition.

Cross-wire calibration studies were also performed. The hot-film probes showed non-linearities in their yaw calibration using Bradshaw's[2] method. As pointed out by Bruun[3], this is due to the fact that the hot-film has a thick quartz substrate with a length to diameter ratio of only about 18. With such a small aspect ratio film, the end effects can have a substantial effect on the lengthwise temperature distribution across the film. Thus, a nonlinear dependence of heat transfer occurs when yawing the probe. A more desirable length to diameter ratio is around 200, the ratio for standard hot-wires. In future tests, a lookup table format will have to be used to calibrate cross-film probes. Also, a more sophisticated method using error correction, Cantwell[4], was written and may be implemented in the next test.

HSCT Test

Trial cross-film measurements were performed on the Boeing HSCT model in the 7-x10-ft. wind tunnel. The purpose of this test was to demonstrate the robustness of the acquisition software and hardware of the hot-film system. A modified simultaneous sample-and-hold device was used to ensure that both wires of the cross-film were sampled at the same time. Unfortunately, a problem caused by the instrumentation cable limited the amount of time spent in the tunnel to three hours. A grid of 20x20 points with half inch spacing was obtained. The resulting velocity map revealed an unexpected flow angularity bias. This was caused by misalignment of the films in the tunnel and performing the calibration outside of the test environment. More detailed measurements of the wake were obtained with a seven hole probe survey.[5] Measurements of streamwise turbulence levels showed the same general trends as static pressure losses.

Cylinder Test

In order to gain more experience with hot-films in a test situation, measurements were taken during a cylinder experiment in the 7x10 ft. wind tunnel directed by Dr. Krothapalli of Florida State University.[6] The purpose of the experiment was to demonstrate drag reduction of a roughened two-dimensional cylinder by placing an airfoil in the near-field wake. The airfoil was placed about 1.05D downstream of the

cylinder and 0.66D off of the centerline (App. A). Reynolds numbers between $1.6x10^5$ and $6x10^5$ were examined. In order to ensure that the cylinder boundary layer was turbulent at separation, the surface of the cylinder was roughened by a knurling process described by Achenbach.[7] This gave a roughness height of about 100 μm and equivalent sand grain roughness k_s/D estimated at $9x10^{-3}$.

One-dimensional traverses were made with a single film across the cylinder wake in the middle of the cylinder span. Output from the hot-film was converted by a LabVIEW program into mean and RMS velocity profiles. The velocity wakes, Fig. 1, show that the total drag of the cylinder is reduced by placing the airfoil in the near-field wake. The mean velocity deficit is less for the case with the airfoil in place. Using seven-hole pressure data, a drag coefficient was calculated using conservation of momentum. The calculated drag coefficient for the cylinder alone was 1.09. Adding the airfoil behind the cylinder wake reduced the total drag coefficient by more than 10% to 0.90.

The pressure distribution of the cylinder was measured by pressure taps around the mid-span. Drag of the cylinder alone was calculated from integration of these pressures over the surface. The drag of the system was determined from the combination of cylinder and airfoil drag. The drag of the added airfoil was estimated from Hoerner[8] using a formula for an elliptical cross section. The airfoil was assumed elliptical because of its large thickness, 33%. Hoerner's formula was assumed to give an upper bound on the drag for the airfoil since it is slightly more aerodynamic than an ellipse. The total drag coefficient of the system was calculated from the pressure measurements to be 1.08 for the cylinder alone and 0.95 for the cylinder with the added airfoil in the wake. The drag for the cylinder with airfoil is 5% higher than that calculated from the velocity profiles. The reason for this discrepancy in drag numbers was a change in calibration of the seven hole pressure probes between runs. The static ring was accidentally switched between runs giving a different reference pressure to the seven-hole probe system. This error was discovered after the test completion and thus the change in reference pressure could not be determined.

An interesting feature of the mean velocity profiles is that they are fairly symmetric in the farfield wake. There is little evidence of the wake of the control airfoil placed in the wake of the cylinder. Examination of a surface pressure profile also shows symmetry around the cylinder itself. This suggests that the added airfoil is a true drag reduction device and does not merely change the direction of the drag force.

The turbulence profiles do have an asymmetrical shape to them. RMS velocities on the airfoil side of the cylinder are less than on the side without the airfoil. Thus, the airfoil must modify the unsteadiness of the vortex shedding without greatly affecting the mean flow. Comparing the wakes to the seven hole probe measurements demonstrated that the turbulence produced was directly related to static pressure losses in the wake. A lower turbulence level resulted in a smaller loss of static pressure. Adding the airfoil decreases the turbulence and static pressure loss in the wake. This again proves the drag is reduced by adding an airfoil to the wake.

The hot-film output was used to check the shedding frequency of the cylinder both with and without the airfoil by running the output of the hot-film through a spectrum analyzer. The output of the analyzer revealed the narrow band resonant frequency of the vortex shedding. When the single film was placed in the wake 7.5 diameters downstream and 0.66 diameters to the right of the cylinder centerline, a Strouhal number of 0.2 was

calculated. It was discovered that the measured shedding frequencies were not affected by the presence of the airfoil and the Strouhal number remained constant around 0.2.

One-Dimensional Traverse

Because the existing traverse in the wind tunnel did not provide adequate access to the top of the wing, a new traverse had to be built in order to access the areas of interest. The first idea was to build a hot-film traverse mounted on the model itself. This was ruled out because of the cost of the modifications to the model and the lack of space to run instrumentation cable. The next best solution was to traverse from the side-wall of the tunnel which corresponded to the top of the wing.

This traverse was to be cantilevered and able to reach as far as the bottom surface of the deflected flap. The traverse consisted of a hollow circular cylinder (1 in. dia.) with an adapter at the end. The adapter allowed any type of Dantec hot-wire mount to be screwed in, single or cross-wire (Fig. 2). The hot-wire mount could be extended an additional four inches in order to reduce the effect of the traverse cylinder on the flow around the hot-film.

Because of the possibility of flow induced vibrations of the cantilevered section with cylindrical cross-section, an airfoil fairing was placed around the cylinder for the first three feet extended from the wall. A nylon bushing at the end of the airfoil section kept the cylinder in the center of the airfoil. Wrapping wire around the cylinder was also considered in order to break the vortex shedding of the exposed cylindrical section. Testing of the wire wrap showed no further decrease of the amount of vibration and was deemed unnecessary. The section of the traverse inside the tunnel is shown in Fig. 3.

The traverse section of the outside of the tunnel, Fig. 4, consisted of a set of guide rails and a lead screw attached to a DC motor. A set of linear bearings attached to a plate was used to attach the traverse cylinder to the guide rails. The pipe fittings holding the traverse cylinder to the plate could be loosened to allow rotation of the hot-film in the flow, giving it effectively two degrees of freedom. A cross-over switch was used to alternate the direction of the current so that the motor could be driven both forward and backwards. Using the switch would drive the cylinder into or out from the test section.

During the flap edge test, a straight single wire was used to take the two dimensional cross-section data. However, the friction bearings of the Dantec probe holders were not strong enough to hold the hot-film in a position parallel to the flow. Thus, a passive aerodynamic fin was placed on the back of the hot-film holder, Fig. 5. The fin proved effective in keeping the hot-film pointed into direction of the mean flow. It was not used in the flap tip region because the size of the fin was on the order of the size of the vortex. The wire would not have remained in a correct orientation with the flow off of the flap edge.

A custom wind tunnel wall section was cut to access various points on the top of the wing. The traverse and airfoil fairing were bolted to the wall at the different locations for measurement. Three different spanwise locations were cut for examining the slat. A long section was cut out of the wall to allow movement along the entire top section of the wing. Finally, a wide section was cut out near the flap edge. For repeatability, positions were marked by tracing the inner tunnel plate on the wall with a wax pen. Repeatability error was estimated to be 1/32 inch.

Positioning error in the traverse was a large concern. It was discovered that the lead screw mechanism had an error of about 1/16" caused by its loose fit in the traverse

which created a backlash. The major positioning error came from a steady-state aerodynamic deflection of the cantilevered cylinder while the tunnel was running. The maximum deflection of the probe was estimated to be 0.25" perpendicular to the traverse plane. This was fairly consistent, however, such that the repeatability error was much less than this. The error mostly affected the absolute position of the probe near the flap edge.

Vibration of the probe was also a concern in the flap edge area. The peak to peak fluctuations of the probe were estimated to be 1/8" when the cylinder was in the core of the vortex. These fluctuations may have also caused false turbulence levels. However, since the measured turbulence levels on the top and bottom of the flap (Figs. 13-15) were nearly equivalent and near freestream turbulence levels (~2%), the errors from false turbulence measurements were deemed negligible.

Even though errors in traverse positioning proved to be dominant near the flap edge, these errors were not critical in the two-dimensional profiles on top of the wing. During these traverses, only the vertical position was crucial. The repeatability of vertical position was within the error range of the traverse - around 1/32 inch. The spanwise and chordwise position were also fairly good - around 1/32" as well. Oscillations of the probe were also considerably less because the traverse was not directly placed in the tip vortex. Also, the small winglet, placed on the probe to control its pitching moment, served to dampen out the aerodynamic vibration. It was estimated that the maximum vibration displacement during the two dimensional traverses was around 1/16". This occurred during measurement behind the flap gap.

In the next test, better relative positioning of the hot-film will be achieved with an electronic touch sensor currently being developed to provide a more accurate starting reference position of the probe near the flap edge. The touch sensor was first successfully implemented by Chow, et. al.[9] Also, the positioning accuracy of the traverse will be improved by removing a large portion of the backlash.

Flap-Edge Test Setup

Measurements were taken in the 7-x10-ft. wind tunnel of NASA Ames Research Center. The model consisted of a NACA 63_2-215 Mod. B main element with a half span 30%c Fowler flap and a 15%c LB-546 slat (App. A).[10,11] Mounted vertically between two false walls, the model had a span of 5 feet and a clean (flap stowed) chord of 2.5 feet. On the main element, boundary layer trip strips were placed at 5% and 10%c on the upper and lower surfaces respectively. The test Mach number remained constant at 0.22 with a Reynolds number based on chord of 3.7 million. The turbulence intensities of the empty test section were measured to be 0.14%, 0.30% and 0.34% for u, v, and w respectively. Approximating a landing configuration, the angle of attack for the wing was fixed at 10° and the flap angle was set to 39°. The slat angle was varied between 6° and 26° and the slat was completely removed for flap edge measurements.

Flap-Edge Measurements

Measurements of the velocities were taken in the three-dimensional flow field of the flap edge as well as in more two-dimensional profiles over the top of the wing itself (App. A).

Temperature variation throughout the tunnel was a problem for the hot-films. A temperature difference of approximately 3° Celsius was measured between the top and

bottom of the tunnel. There were also pockets of hot and cold spots in the same position of the tunnel which varied at most 1.5° Celsius. Temperature variation between the center of the vortex and the surrounding flow was also considered a problem. Taking this into consideration, a linear temperature dependence was included in both the calibration and acquisition software. A thermocouple was placed behind the hot-film in the flow and the temperature was recorded at every data point.

The sample period for all measurements was kept constant at 20 seconds. The sampling rate was 1000 Hz. The period was long enough to obtain a fairly stable mean in very turbulent flow and also obtain accurate RMS velocities. The raw hot-film signal was passed through an anti-aliasing filter with a cutoff frequency of 50 kHz and a roll-off rate of 18 dB/decade.

Time-dependent data was necessary for correlation with unsteady pressure transducers and wall microphones. However, only the AC coupled signal was needed. The hot-film signal was passed through a high pass filter with a DC cutoff frequency of 1 Hz and a roll-off rate of 18 dB/octave. This signal was then recorded on a digital tape along with the signals of 14 Endevco pressure transducers and one wall microphone. The sample rate of the tape recorder was set at 80 kHz with its anti-aliasing filter set at 20 kHz. These numbers were chosen by examination of previous measurements of full-scale aircraft acoustics.[12] Nothing above 20 kHz was deemed acoustically interesting, once scaled to commercial aircraft sized wavelengths. The hot-film probes were tuned to a frequency response of approximately 50 kHz (at 100 m/s). Thus, all frequencies up to 25 kHz were accurately captured by the hot-film probe. The digital recorded tape was later played back and analyzed on a spectrum analyzer. Correlations were made between the hot-film and the unsteady pressure sensors, and results from those studies along with acoustic spectra were issued in a NASA CDTM.[13]

Results from the Top of the Wing Measurements

The two-dimensional profiles over the top of the wing proved to be most interesting. Four different configurations were examined: no slat, 10° slat deflection, 20° slat deflection and an acoustically modified slat with a 20° slat deflection. The actual slat deflection angles were closer to 6° and 26° respectively. The slat gap was fixed at 2% of wing chord. The overlap was -0.5%c.

The traverse at 0.66 of the slat chord, Figure 6, shows that the mean velocities remain relatively unchanged over the slat when varying the slat angle. However, the 6° slat case shows slightly higher turbulence levels. This is because the relative position of the probe is different between the 26° slat and the 6° slat. For the measurements of the 26° slat, the probe is actually farther back chordwise on the slat than 6° slat. Both of these turbulence levels are the order of the freestream turbulence ~1%.

Traverses just behind the slat gap, 0.05 of the main chord, Figure 7, show a difference in velocity profiles between configurations. The mean velocities of the 26° slat case are nearly 10% higher than the 6° slat case near the surface of the wing. Also, the no slat case has the highest velocities of all: 5% greater than the 26° slat. This is consistent with surface pressure plots of the 6° and 26° slat which show the 26° slat has a higher pressure peak on the main element. The 26° slat gap flow has a much higher jet velocity than the 6° slat and therefore a higher main element pressure peak. Repeated runs showed that turbulence levels were relatively independent of the slat deflection. The wake of the slat can be seen in all of the mean velocity profiles as well as the turbulence levels.

Velocity profiles near the center of the main element, Figure 8, show close similarity in all model configurations. There is slight evidence of the slat wake with a deficit in the mean velocity and an increase of the turbulence levels at about 0.04 chord lengths from the surface. This is more pronounced in the 6° slat than the others. The reason for this is explained below.

Mean velocities near the main trailing edge, Fig. 9, are once again fairly similar. Again, the 6° slat wake velocity deficit is slightly larger than the 26° slat wake.

The effect of slat deflection is much more pronounced in the wakes behind the flap gap. Figure 10 shows the velocity profiles at 0.16 of the flap chord where there are appreciable differences in velocities. The slat wake can be seen in all of the slat configurations around 0.08 chord lengths from the surface. It is most pronounced for the 6° and basic 26° slats. As seen in the figure, a higher slat deflection angle produces a lower velocity deficit in the wing wake. This is likely because the slat increases the camber of the wing producing a larger adverse pressure gradient on the backside of the wing. Therefore, the flow over the top of the wing is decelerated to a greater amount than with a lower slat deflection angle. It was also noticed that the acoustically modified slat configuration has slightly less velocity deficit from the top of the wing than the basic slat. This is likely cased by the modification increasing the turbulence in the boundary layer. The more turbulent boundary layer is less affected by the adverse pressure gradient and maintains a more robust profile. The lesser evidence of a slat wake is also due to increased mixing between the slat wake and wing boundary layer. The turbulence profile of the no slat case shows abnormally high turbulence levels outside of the wake. This was caused by a faulty wire introducing electrical fluctuations into the system. The wire was quickly replaced, but time constraints did not permit a repeat run.

Just past half chord of the flap, Figure 11, the velocity profiles are similar again. Velocities for the 26° slats are again slightly lower because of the greater adverse pressure gradient. The 26° slats have higher turbulence levels in the wing wake. All slat configurations show the wake of the slat starting at 0.01 chord lengths from the surface and ending at about 0.15 chord lengths from the surface.

The final two dimensional velocity profiles, Figure 12, were taken at the trailing edge of the flap. These profiles again show very good agreement with the previous data. The 26° slat configuration has lower velocities and higher turbulence levels. The basic 26° slat was separated, as evidenced by 80% turbulence levels, in the wake. This was probably induced by the hot-film probe or traverse at the trailing edge. Previous runs without the hot-film did not indicate any kind of separation. The acoustically modified 26° slat did not separate. This demonstrates that the modifications increased the turbulence in the boundary layer and helped prevent separation.

An interesting phenomena occurs in all turbulence profiles over the flap. The 26° slats have higher turbulence levels in the wing wake, while the 6° slat has lower turbulence levels than even the no slat case. The reasons for this are not fully understood. One possible reason is that the 6° slat is configured such that the jet velocity and the flow velocity over the top of the slat are nearly equal, Fig. 7. Therefore, the turbulence created in the shear layer of the slat gap is not as great.

Results from the Flap-Edge Measurements

The three-dimensional flow region of the flap edge was much harder to measure accurately with a single wire, as made evident by the wide scatter in the data. However,

trends in the data do reflect some of the flow physics. A single wire with a 90° bend, Fig. 2, was used for measurements in this region. The probe was oriented such that it would measure the freestream velocity assuming no sideslip. The probe could be rotated to measure velocity in a plane parallel to the wing chord. However, any out of plane velocities could not be measured directly even though they did affect the hot-film output. At each measurement point, the probe was rotated by hand to the point of maximum velocity. This done by reading the point of maximum hot-film voltage output with a voltmeter. Ideally, a traverse which could pitch and yaw the probe would allow for complete nulling of the film, resulting in more accurate results. However, such a traverse would be prohibitively expensive and was thus ruled out as a solution for further tests.

Hot-film traverses were made in relation to unsteady pressure transducers on the flap edge. The zero location was directly to the side of the flap edge transducers about 3/8" measured perpendicularly off of the side face. Traverses were then made in a line perpendicular to the wing chord on both the top and bottom of the flap (App. A). Three different chordwise positions were examined at 40%, 53%, and 68% of the flap chord. Measurements were taken on two different flap configurations: the standard composite Fowler flap and a flap designed by Revell for noise suppression.[14]

Figure 13, shows the velocity profiles at 40% of the flap chord. It is obvious that the point of maximum total velocity is at the flap tip (zero on the plot). The point of minimum mean velocity corresponds to the wake of the main element. Examining the turbulence levels shows a similar two peak pattern. The point of maximum turbulence is the main element wake. A much smaller peak at the flap edge indicates that the vortex rollup over the edge is fairly steady in this area. Comparison between the baseline flap and acoustically-treated flap tip show very little difference in mean flow or turbulent fluctuations.

Figure 14 displays the velocity profiles slightly farther downstream at a location of 53% of the flap chord. The mean velocity shows a similar pattern of low velocity in the wake of the main element and a high velocity at the flap edge. There is also good agreement between the baseline flap and acoustically-treated flap mean velocity profiles. Plots of the turbulence intensity show a slight difference between the two configurations. Both show a high peak at the flap edge. However, the baseline flap has a much higher peak turbulent intensity of 15%, compared to only 5% for the acoustically-treated tip.

Figure 15 shows velocity profiles further downstream at 68% of the flap chord. Here the difference between the acoustically-treated and baseline flap tips is more pronounced. The mean velocity at the baseline flap tip reaches a peak similarly to the previous profiles. However, the acoustically-treated flap mean velocity increases near the flap edge and then levels off. This plateau continues for a couple of main chord percentages and then increases again to a lower level than the baseline tip peak. The mean velocity of the acoustically-treated tip then seems to follow the profile of the baseline tip once past the influence of the flap. The turbulence levels are also significantly different. The peak of the acoustically-treated flap profile is over twice as high as that of the baseline flap. These facts suggest that the acoustically-treated flap actually modifies the vortex structure around the flap edge.

One final conclusion made from these plots is that the vortex does not follow the flap edge. Its center corresponds to the point of maximum mean velocity and moves farther away from the flap edge as it convects downstream. This observation is consistent with the flow visualization studies of the wing.

Five-hole Probe

In the next test, mean velocity profiles measured by the hot-film will be verified using a five-hole probe. This was deemed necessary because hot-films are less accurate for mean velocity measurements than for turbulence measurements. A five-hole probe fitting was constructed for the one-dimensional hot-film traverse. Using the same traverse will allow the five-hole probe to take measurements at the identical locations where hot-film measurements were made. However, since five-hole probes are fairly sensitive to flow-field turbulence levels, their use around the turbulent flap edge may be restricted.

Particle Image Velocimetry

From May to August 1997, time was spent learning about Digital Particle Image Velocimetry (DPIV or simply PIV) at Florida State University under the direction of Professor Luiz Lourenco. Several small studies were performed using PIV to measure the mean and turbulent velocities of a subsonic jet as well as the turbulent spectra of the jet flowfield. All results presented here where done in conjunction with Bahadir Alkislar, a graduate student of Prof. Lourenco.

Figure 16 shows a sample image of a subsonic jet with velocity vectors calculated over a small region of the flow below the centerline of the jet. The jet width was 1 cm and was run at a Reynolds number of 11400. The velocity vectors superimposed on this image were produced using a cross-correlation method between two images taken only a few microseconds apart.[15,16] Image pairs (and hence velocity vectors) could be produced at a maximum rate of 15 Hz. This limit was set by both the download speed of the cameras and also the repetition rate to the laser illumination. At this rate, multiple velocity fields could be gathered for time averaging over the entire field or examination of the propagation of large scale structures in the flow.

Using PIV to gather velocity spectra is a new technique developed by Professor Lourenco and his graduate students. The spectral PIV method is a simple extension of basic DPIV to the measurement of high-frequency fluctuations. It requires the use of two independently functioning PIV systems in which the cameras and laser sheets of both systems operate in the same measurement plane. By delaying one laser and camera system from the other, very short time variations in the velocity field can be realized. Changing the time delay between the independent PIV systems results in a map of the velocity field as a function of time. The circulation at any point can be calculated by integrating velocity vectors along a box surrounding the point. This circulation value can then be correlated as a function of the time delay between systems. Finally, a spectra of the circulation fluctuation at the point can be obtained through a Fourier Transform of the correlation data. A more accurate estimate of the correlation is obtained by averaging over a large number of correlation values at each time delay.

For example, by integrating around a 3x3 velocity vector grid (Fig. 16), the circulation around a single point in the flow (x/d=1.5, y/d=-0.5) was calculated for each image's vector field. After this calculation, cross-correlations between the delayed and undelayed circulation values were made. Finally, an average correlation over 30 values for each time delay was generated. Figure 17 is a plot of the average circulation cross-correlation as a function of time delay. As seen in the figure, there is a large frequency oscillation in the correlation plot. The frequency of this oscillation was calculated by taking the Fast Fourier Transform of the correlation function. This is shown in Figure 18.

As expected, there is a large peak in the peak in the spectra at 1543 Hz, which is near the predicted natural shedding frequency of the jet for this Reynolds number.

In the third flap-edge test, the spectral PIV technique will provide an additional source of flowfield spectra measurement of the slat flow. The PIV measurement technique has an advantage over single-point measurement techniques such as the hot-wire and LDA in that it can examine the entire flowfield instantaneously. The new spectral PIV technique will provide instantaneous velocities of the slat cove flow, and also provide an unsteady velocity spectrum for up to 65,000 independent points in the flow. Measurement of whole flowfield spectra will allow for examination of spatial variation of velocity fluctuations and provide new insight into the unsteady flow around high-lift systems.

The spectral PIV method provides an incredible amount of useful data, which inherently creates a new set of challenges. The greatest challenge for the spectral technique involves storage of the PIV images for future analysis. For reasonable statistical accuracy (2% of the standard deviation), 1000 velocity vector fields must be collected per camera at each time delay between the two independent lasers (i.e. single frequency point on the spectra). Each velocity vector field requires 2 images from its respective camera. Therefore, in order to obtain a 1 kHz resolution spectra across a bandwidth of a 25 kHz spectra, 100,000 images are necessary. With each image taking up 1M of memory, a total of 100 Gbytes of memory must be used to obtain the spectra for a single test configuration. With compression routines, the amount of storage capacity can be reduced to approximately 68 Gbytes. In order to calculate spectra for 6 different model configurations, over 400 Gbytes of compressed images must be stored. Storage will be provided by NASA Ames mass storage group who will make space available on their 3.2 Tbyte tape drives. However, data transfer rates to the tape drives through a basic Ethernet connection may limit the amount of data that can be stored during the test.

Upon returning to NASA Ames in August, a buildup of hardware components for using spectral PIV in the 7-x10-ft. wind tunnel was started. (App. B) This included designing and building an optical traverse for the laser table which can create, align and reflect two independent laser sheets to any position in the tunnel. In addition, a box which holds the two cameras necessary for the spectral PIV inside the tunnel was designed and built. The box contains mirrors and beam splitter optics necessary for both cameras to separately image an identical measurement plane in the slat cove. Also, in order to provide optical access to the slat cove, a window was placed on the top ground plane between the model and the ceiling of the wind tunnel. The design of these three components was critical because precise alignment of the cameras and laser sheets in the slat cove is necessary for good accuracy using this spectral measurement technique.

Conclusions

The HSCT test revealed that more research will have to be done on using cross-film probes. An alternate calibration method will be used and a more effective method of placing the probes in the direction of the flow must be implemented.

The cylinder test demonstrated that the drag of a cylinder can be reduced by placing an airfoil in the near-field wake. Mean velocity data from the hot-film can be used in conjunction with static pressure data of the wake to produce reasonable drag coefficients.

Measurements of the quasi-two-dimensional flow over the top of the wing revealed a great influence of the slat deflection. The slat wake could be seen in all

velocity profiles and continued over the flap. Higher slat deflections produced a higher jet flow speed through the slat gap. This resulted in a greater suction peak on the main element. The acoustically-treated slat increased the turbulence in the boundary layer. This made the wing less likely to separate and increased flow velocities over the flap.

Measurement of the three dimensional flow about the flap edge was difficult to resolve with a single wire. Trends in the data indicate the flap tip is a local point of maximum velocity and turbulent intensities. The Revell flap tip used for acoustic damping changed the structure of the vortex around the flap edge. Further studies will be made to further map out this region's velocities and turbulence.

Uncertainty of the position near the flap edge was not at all reasonable. For the next phase of the test a new traverse mechanism will have to be used. An electronic touch sensor to find the surface of the wing while the tunnel is running will be implemented. Aerodynamic deflection of the traverse can then be trimmed by moving the traverse back to the desired position near the surface. Ideally, a three-dimensional traverse would traverse the probe to any position on the edge. The probes could then be oriented in a direction which would reduce their error from cross-flow velocity components. However, such a system was deemed prohibitively expensive and hence ruled out as an option. Instead, mean velocity profiles from the hot-film will be verified using a five-hole probe. This will also result in a better understanding of the flow angularity in this complicated flow region. However, since five-hole probes are fairly sensitive to flow-field turbulence levels, their use around the turbulent flap edge may be restricted. Further study on the accuracy of the five-hole probe results will have to be performed.

The technique of particle image velocimetry (PIV) was used to study the steady and unsteady behavior of a subsonic jet at Florida State University. Mean velocity measurements were made using a cross-correlation PIV method. A newly developed spectral PIV technique was used to measure the spectra of unsteady shedding in the subsonic jet. The measured frequency was very close to the predicted shedding frequency of the jet running at an identical Reynolds number.

This spectral PIV method will be used to measure steady an unsteady flow through the slat cove in the next flap-edge test. Hardware was built to accommodate the spectral PIV technique in the 7-x10-ft. wind tunnel. PIV has an advantage over single-point measurement techniques such as the hot-wire and LDA in that it can measure velocity and spectra of the entire flowfield instantaneously. Along with this advantage, comes the pricetag of storing massive amounts of data, up to 100 Gbytes of information per configuration during the flap-edge test. This disk space is being provided NASA Ames mass storage group. However, data transfer rates may still limit the amount of data that can be saved during the test.

Support for this research has continued through a NASA Graduate Student Program Fellowship which started in July 1996 and will end in June 1999. The thesis should be completed by this time.

References

[1]Watmuff, J. H., "A high-performance constant-temperature hot-wire anemometer," NASA CR-177645, MCAT Inst., 1994.

[2]Bradshaw, P. "Cross-wire probe calibration," Heat Transfer and Turbulence Mechanics Group, M.E. Dept., Stanford University, Stanford, CA, July 1992.

[3]Bruun, H. H., Hot-wire Anemometry - Principles and Signal Analysis, Oxford Science Publications, New York, 1995.

[4]Cantwell, B. "A flying hot-wire study of the turbulent near wake of a cylinder at a Reynolds number of 140,000," Graduate Aeronautical Laboratories, California Institute of Technology, Pasadena, CA, 1976.

[5]Takahashi, T.T., Eidson, R.C. and Heineck, J.T. "Aerodynamic Characteristics of a Supersonic Transport with Pneumatic Forebody Flow Control," AIAA Paper 97-0043, 1997.

[6]Krothapalli, Shih, C., A., Lourenco, L. M., Walker, S., Moriarty, P., "Drag Reduction of a Circular Cylinder at High Reynolds Numbers," AIAA Paper 97-0211, 1997.

[7]Achenbach, E., and Heinecke, E., "On vortex shedding from smooth and rough cylinders in the range of Reynolds numbers $6x10^3$ to $5x10^6$," *Journal of Fluid Mechanics*, 1981, pp. 109, 239-251.

[8]Hoerner, S. F., Fluid Dynamic Drag, Hoerner Fluid Dynamics, Albuquerque, NM 87120, 1965, pp. 3-1 - 3-28.

[9]Chow, J. S., Zilliac, G. G., Bradshaw, P., "Turbulence measurements in the near-field of a wingtip vortex," ASME Forum on Turbulence in Complex Flow, Nov. 6-11, 1994, Chicago, Illinois.

[10]Storms, B. L., Takahashi T. T., Ross, J. C., "Aerodynamic influence of a finite-span flap on a simple wing," SAE Technical Paper Series - 951977, 1995.

[11]Mathias, D. L., Roth, K. R., Ross, J. C., Rogers, S. E., Cummings, R. M., "Navier-Stokes analysis of the flow about a flap edge," AIAA Paper 95-0185, 1995.

[12]Sen, R., Blackner, A., Yee, P., Stoker, R., "Airframe Noise Generation and Radiation," Contract NAS1-20090 Task 2, NASA Langley Research Center, Hampton, VA, January, 1997.

[13]Moriarty, P. J., Storms, B. L., Ross, J. C., Horne, W. C., Dougherty, R. P., "Acoustic and Turbulent Coherence Measurements on a Leading-Edge Slat," NASA CDTM 21-003, NASA Ames Research Center, Moffett Field, CA, August 1997.

[14]Revell, J., Kuntz, H., Balena, F., "Airframe trailing edge flap noise reduction by porous acoustic treatment," 3rd AIAA/CEAS Aeroacoustics Conference, Atlanta, GA, May, 1997.

[15]Keane, R. D., Adrian, R. J., "Theory of Cross-Correlation Analysis of PIV Images," *Applied Scientific Research*, Vol. 49, pp. 191-225, 1993.

[16]Lourenco, L. M., "Particle Image Velocimetry," Von Karman Institute for Fluid Dynamics, Lecture Series 1996-03, June 3-7, 1996.

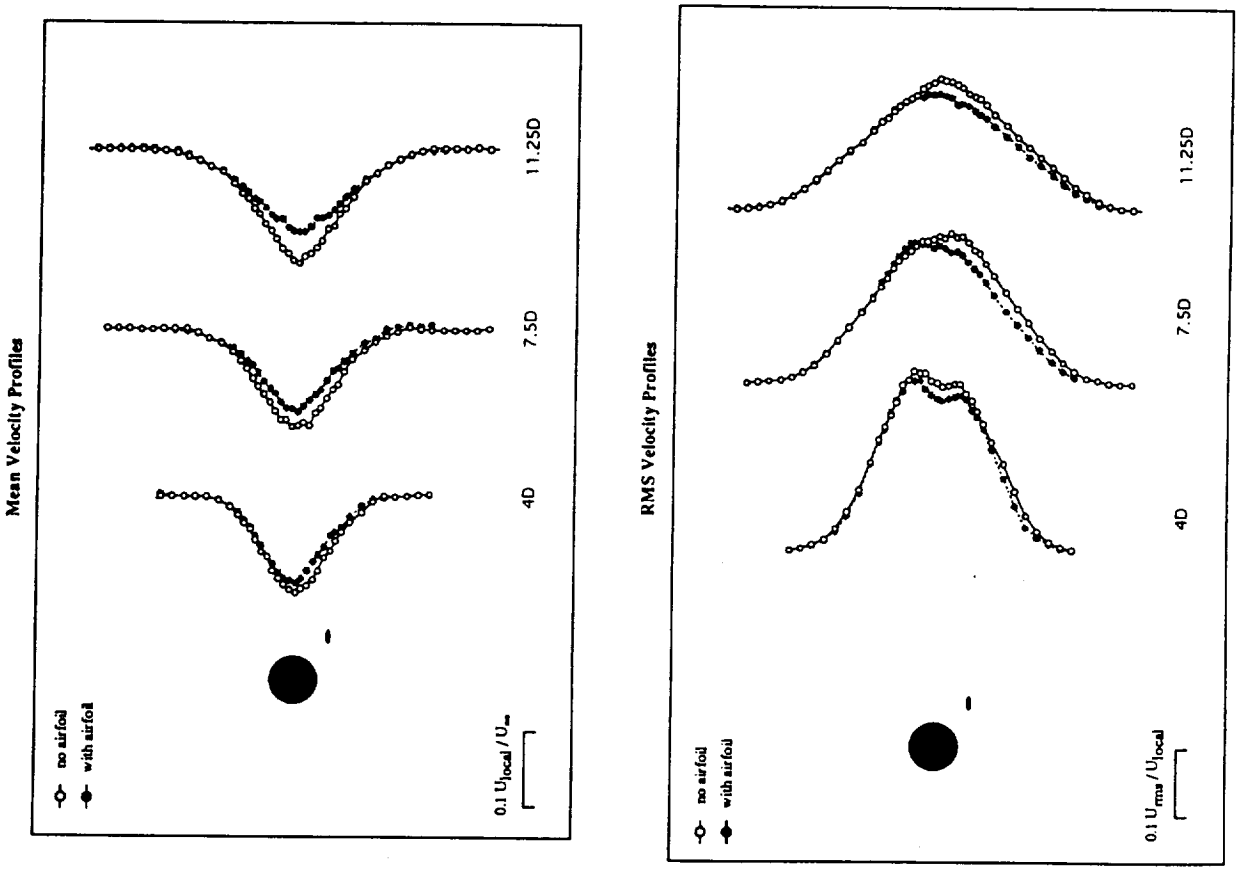

Figure 1. Cylinder Velocity Profiles

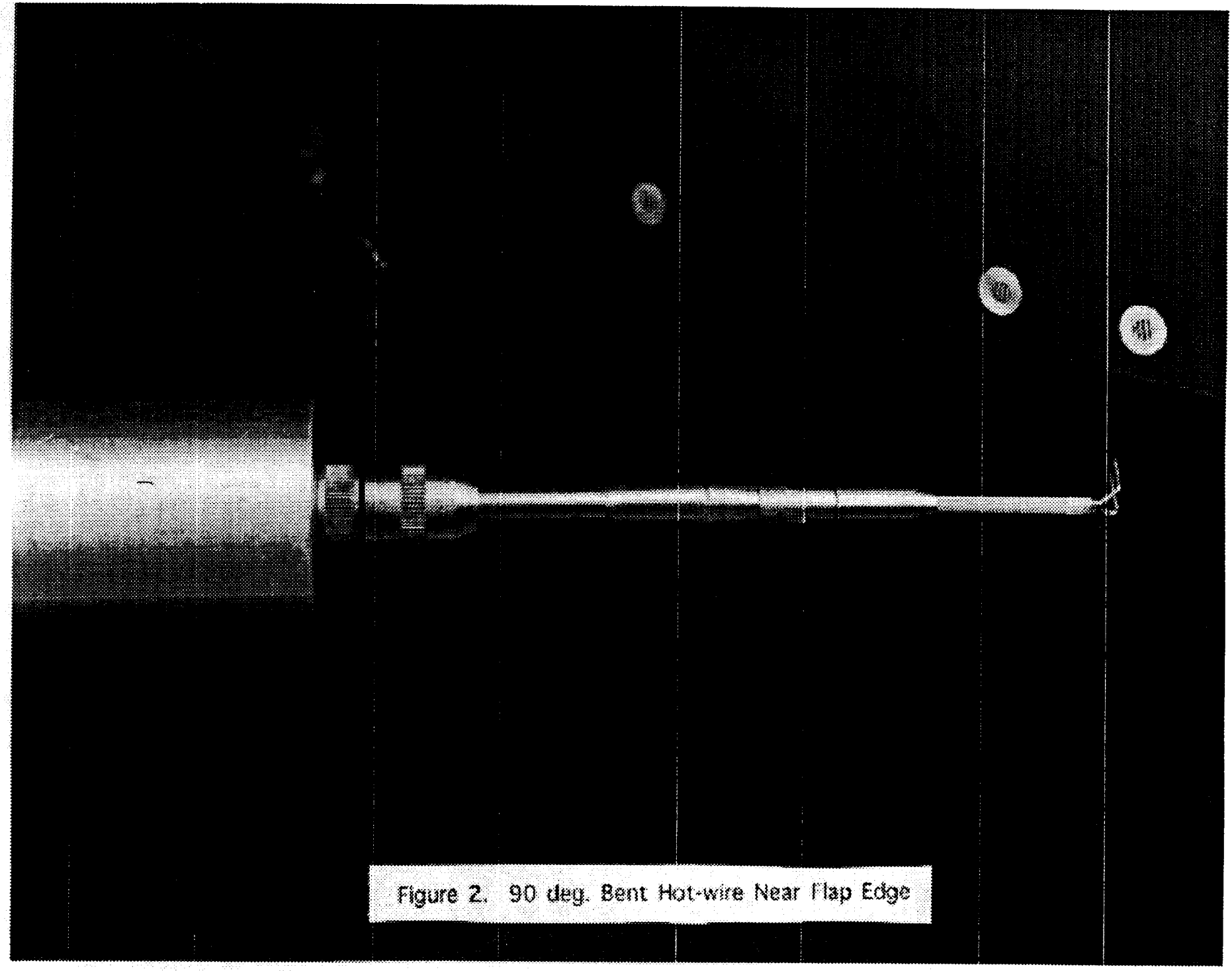

Figure 2. 90 deg. Bent Hot-wire Near Flap Edge

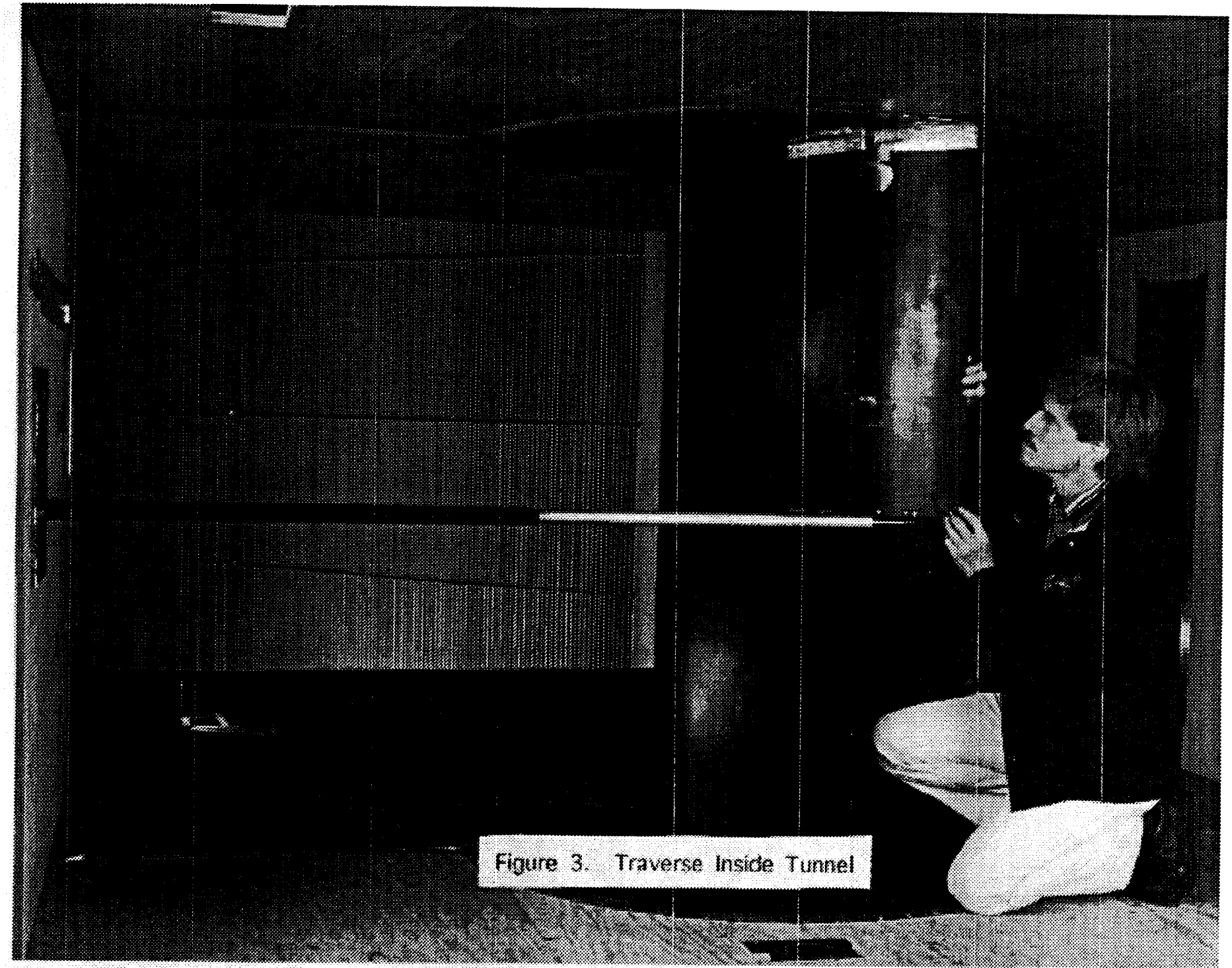

Figure 3. Traverse Inside Tunnel

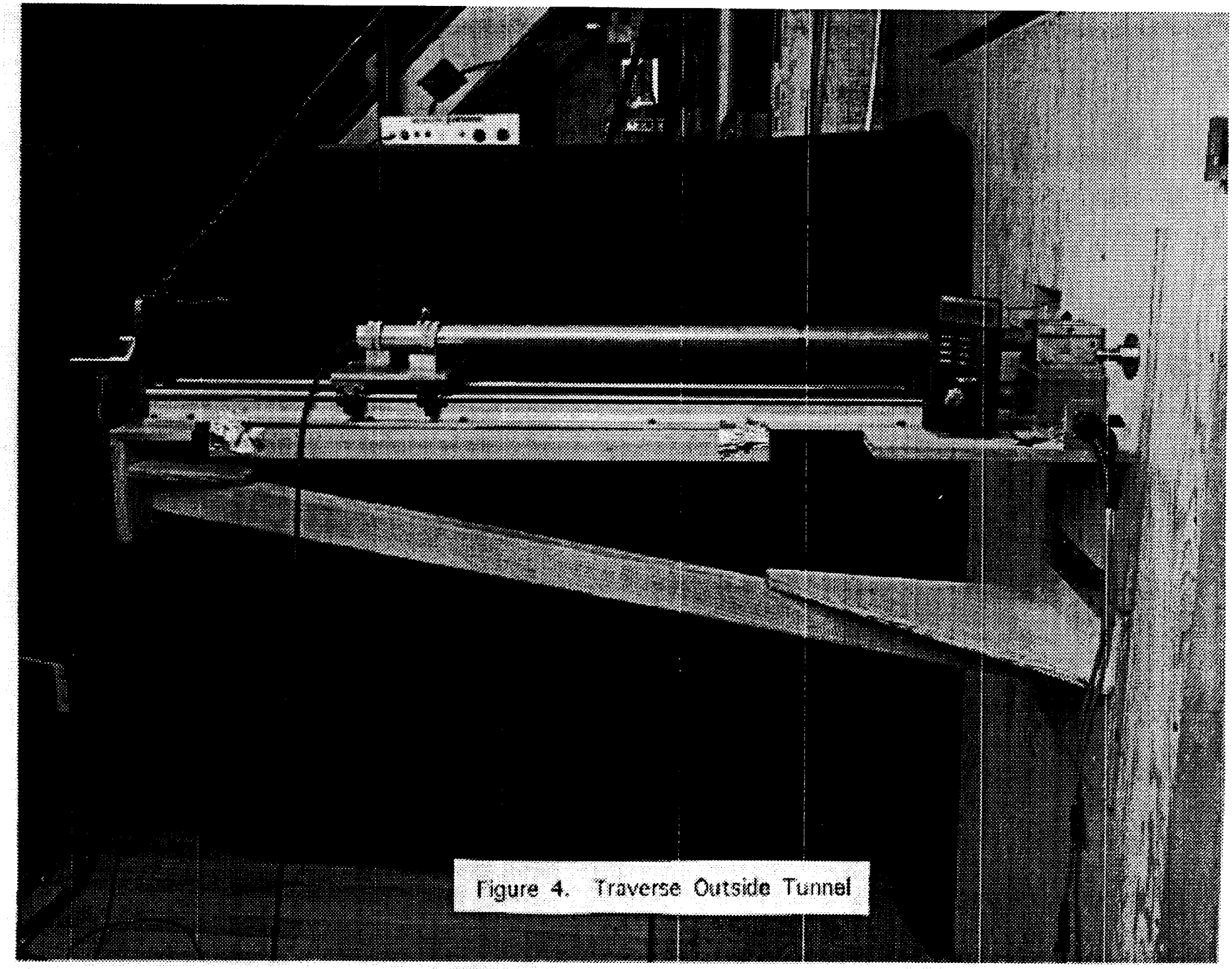

Figure 4. Traverse Outside Tunnel

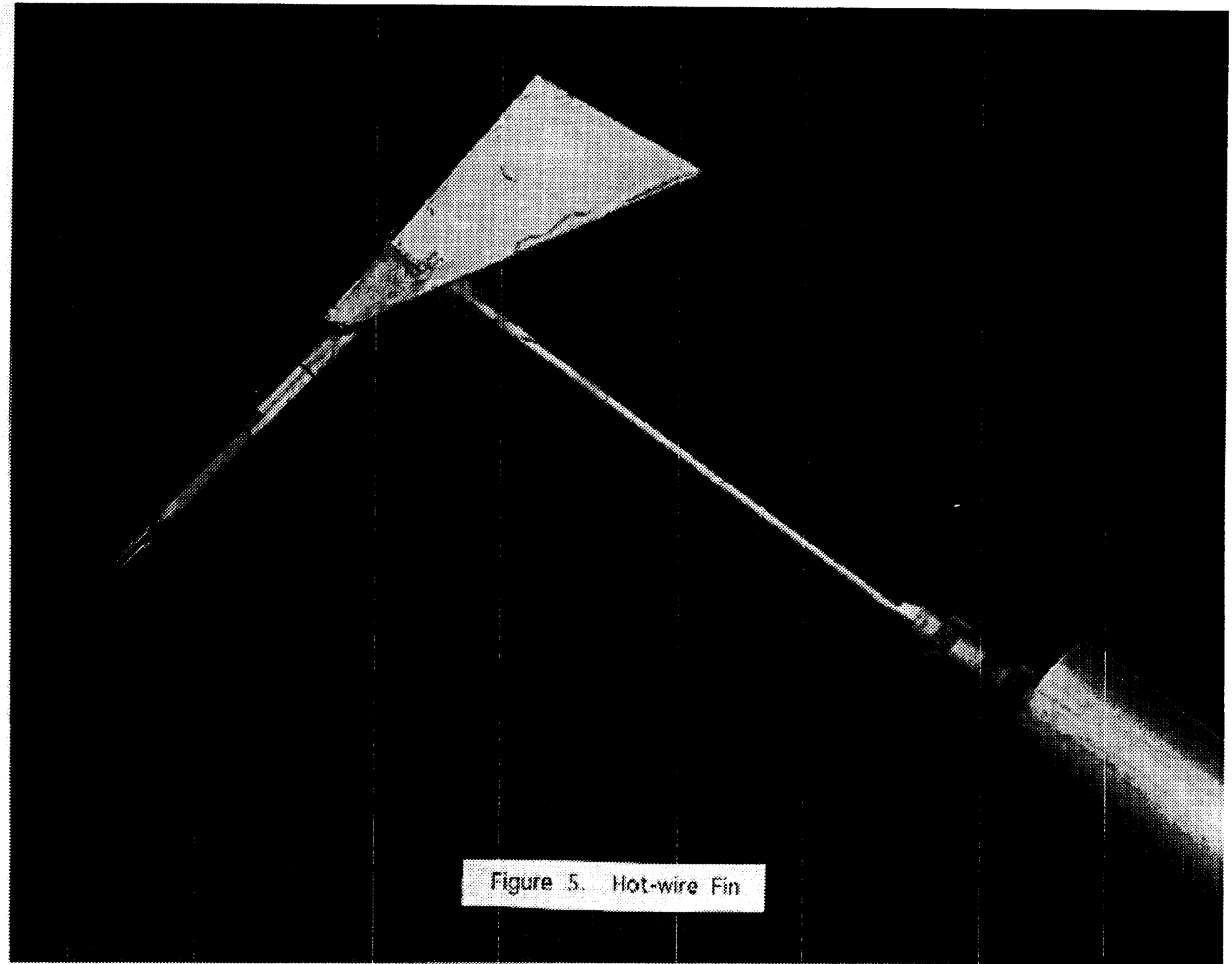

Figure 5. Hot-wire Fin

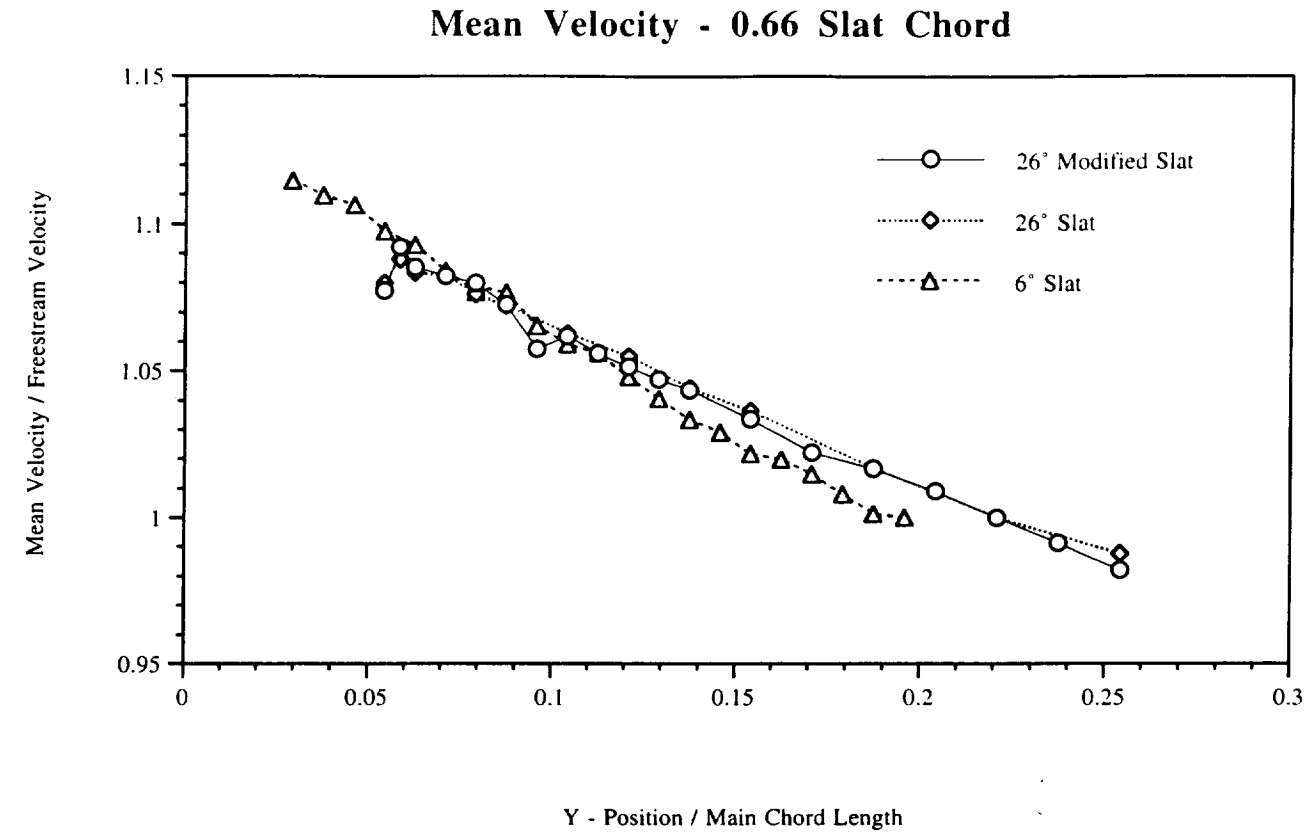
Mean Velocity - 0.66 Slat Chord
Mean Velocity / Freestream Velocity
1.15
1.1
1.05
1
0.95
0
0.05
0.1
0.15
0.2
0.25
0.3
26° Modified Slat
26° Slat
6° Slat
Y - Position / Main Chord Length

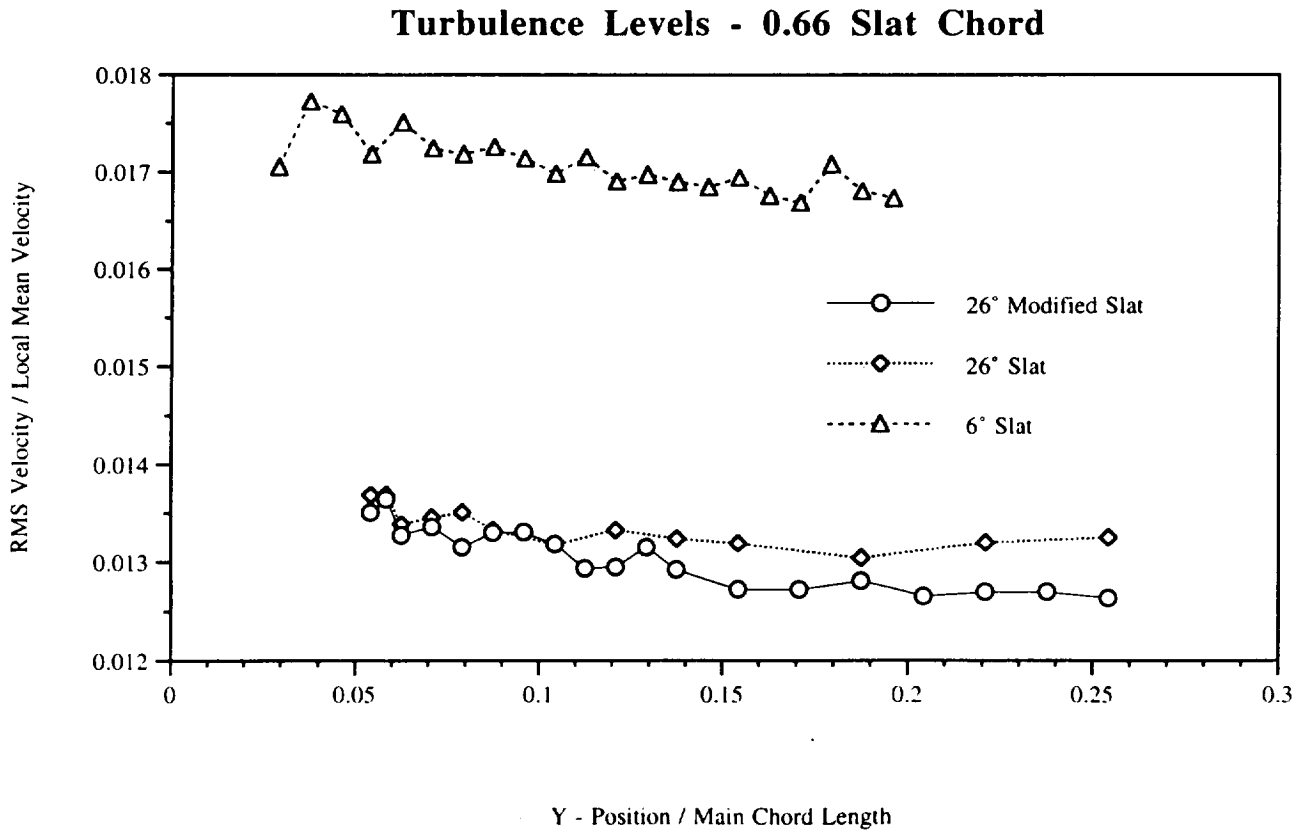
Turbulence Levels - 0.66 Slat Chord
RMS Velocity / Local Mean Velocity
0.018
0.017
0.016
0.015
0.014
0.013
0.012
0
0.05
0.1
0.15
0.2
0.25
0.3
26° Modified Slat
26° Slat
6° Slat
Y - Position / Main Chord Length

Figure 6

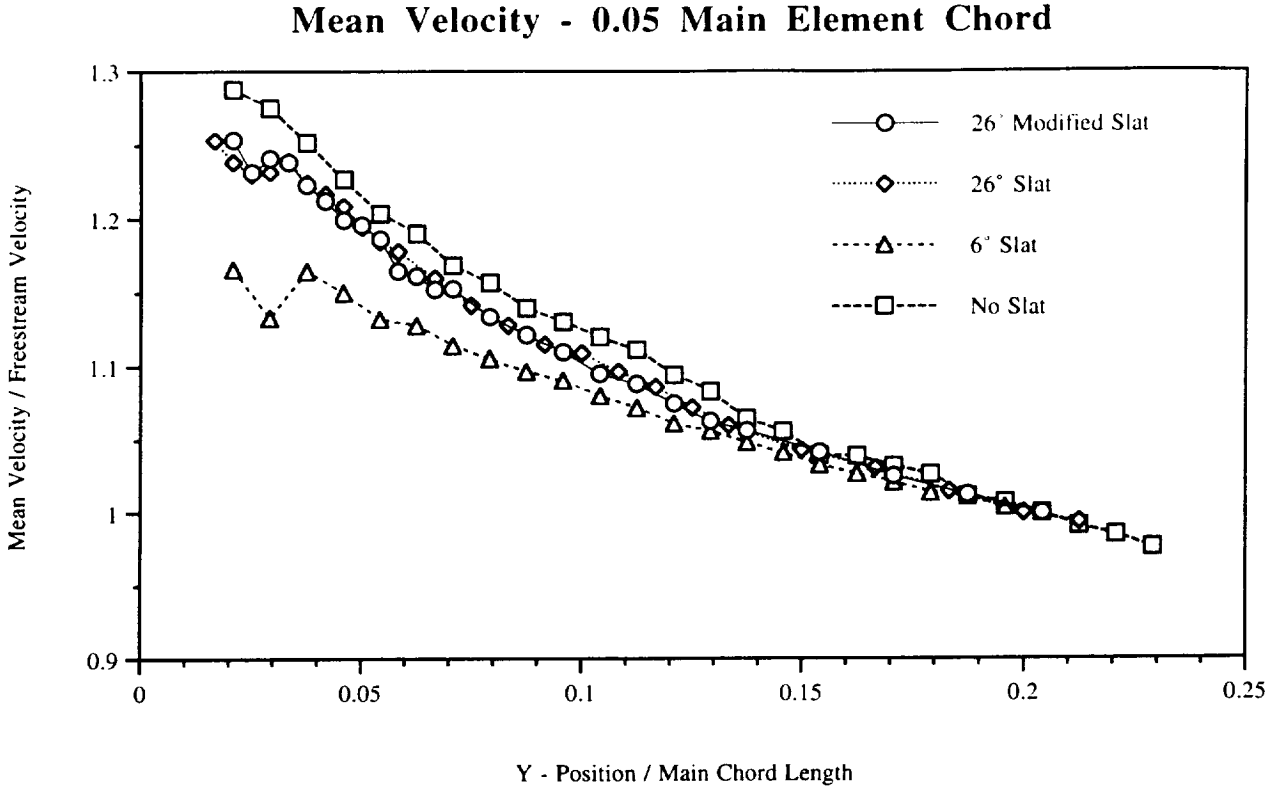
Mean Velocity - 0.05 Main Element Chord
Mean Velocity / Freestream Velocity
1.3
1.2
1.1
1
0.9
0
0.05
0.1
0.15
0.2
0.25
Y - Position / Main Chord Length
26° Modified Slat
26° Slat
6° Slat
No Slat

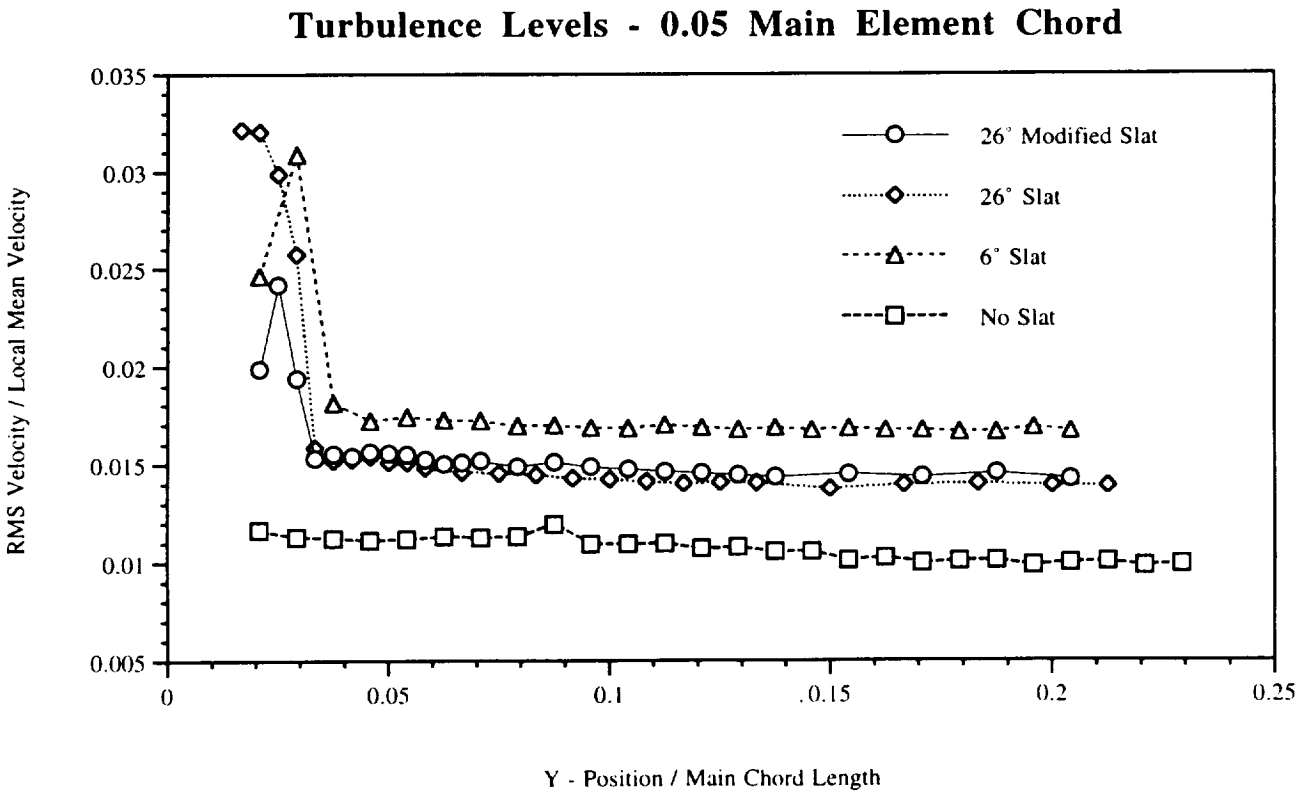
Turbulence Levels - 0.05 Main Element Chord
RMS Velocity / Local Mean Velocity
0.035
0.03
0.025
0.02
0.015
0.01
0.005
0
0.05
0.1
0.15
0.2
0.25
Y - Position / Main Chord Length
26° Modified Slat
26° Slat
6° Slat
No Slat

Figure 7

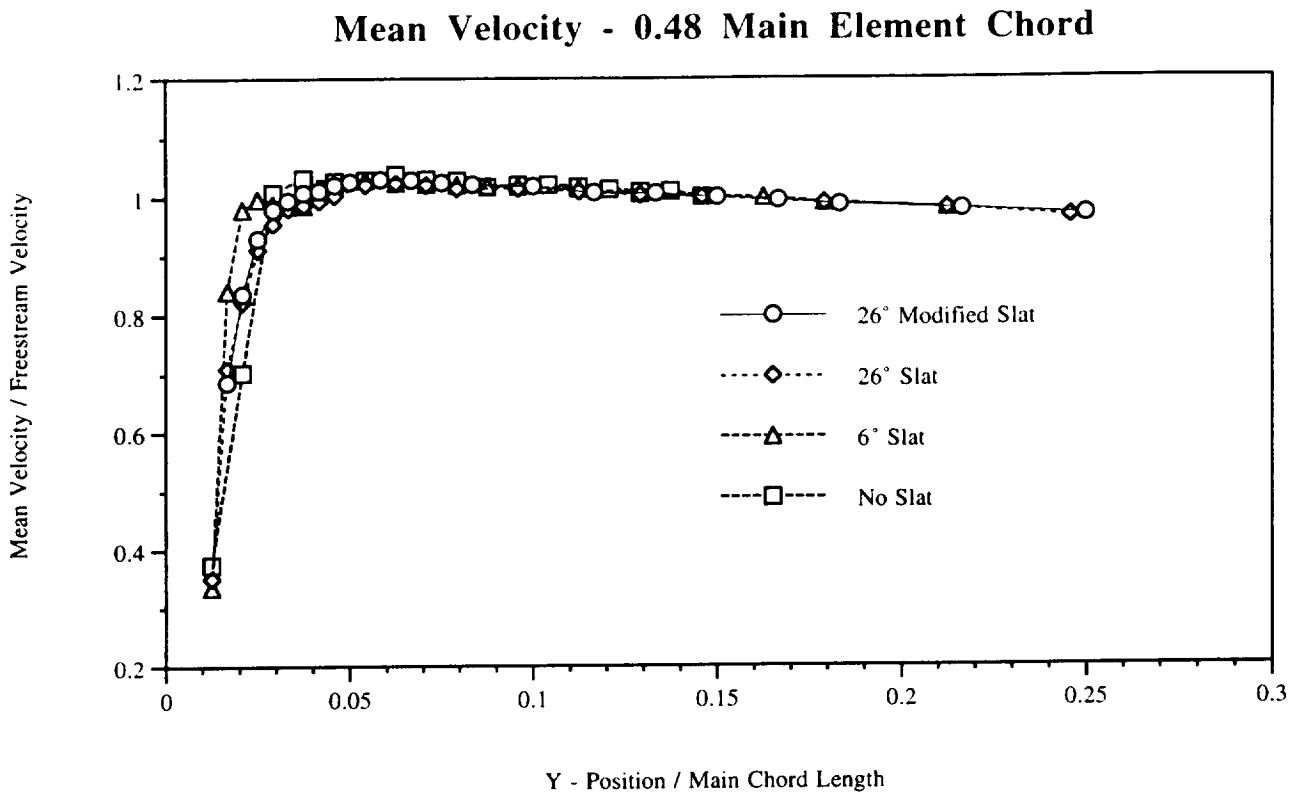
Mean Velocity - 0.48 Main Element Chord
Mean Velocity / Freestream Velocity
1.2
1
0.8
0.6
0.4
0.2
0
0.05
0.1
0.15
0.2
0.25
0.3
26° Modified Slat
26° Slat
6° Slat
No Slat
Y - Position / Main Chord Length

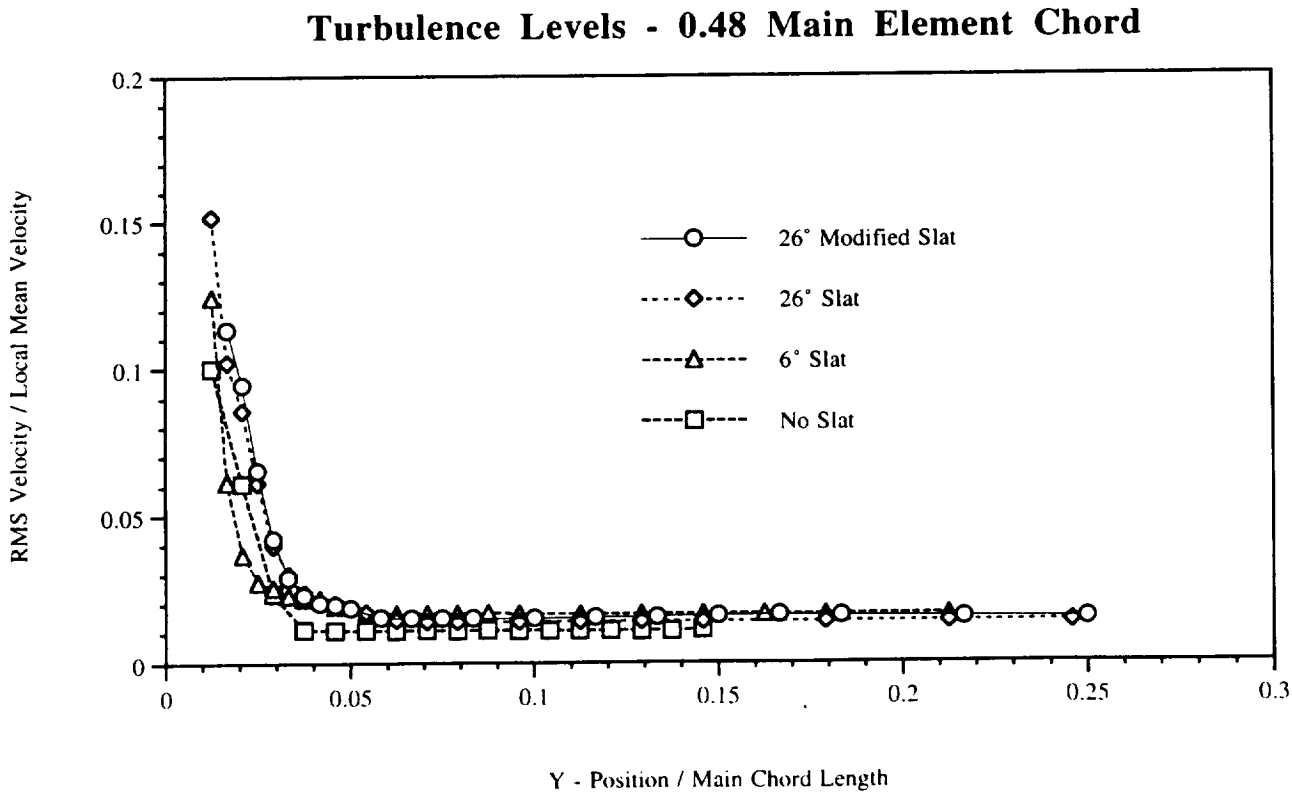
Turbulence Levels - 0.48 Main Element Chord
RMS Velocity / Local Mean Velocity
0.2
0.15
0.1
0.05
0
0
0.05
0.1
0.15
0.2
0.25
0.3
26° Modified Slat
26° Slat
6° Slat
No Slat
Y - Position / Main Chord Length

Figure 8

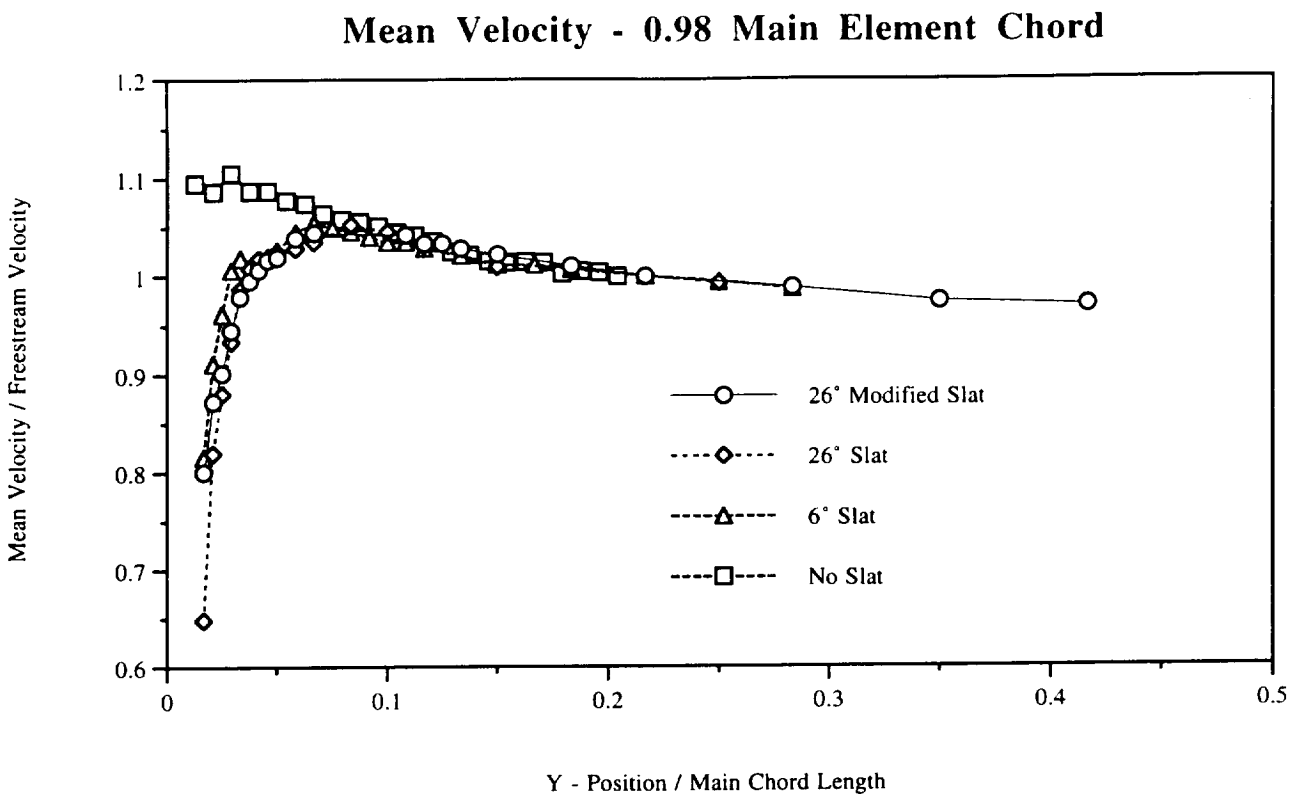
Mean Velocity - 0.98 Main Element Chord
Mean Velocity / Freestream Velocity
1.2
1.1
1
0.9
0.8
0.7
0.6
0
0.1
0.2
0.3
0.4
0.5
26° Modified Slat
26° Slat
6° Slat
No Slat
Y - Position / Main Chord Length

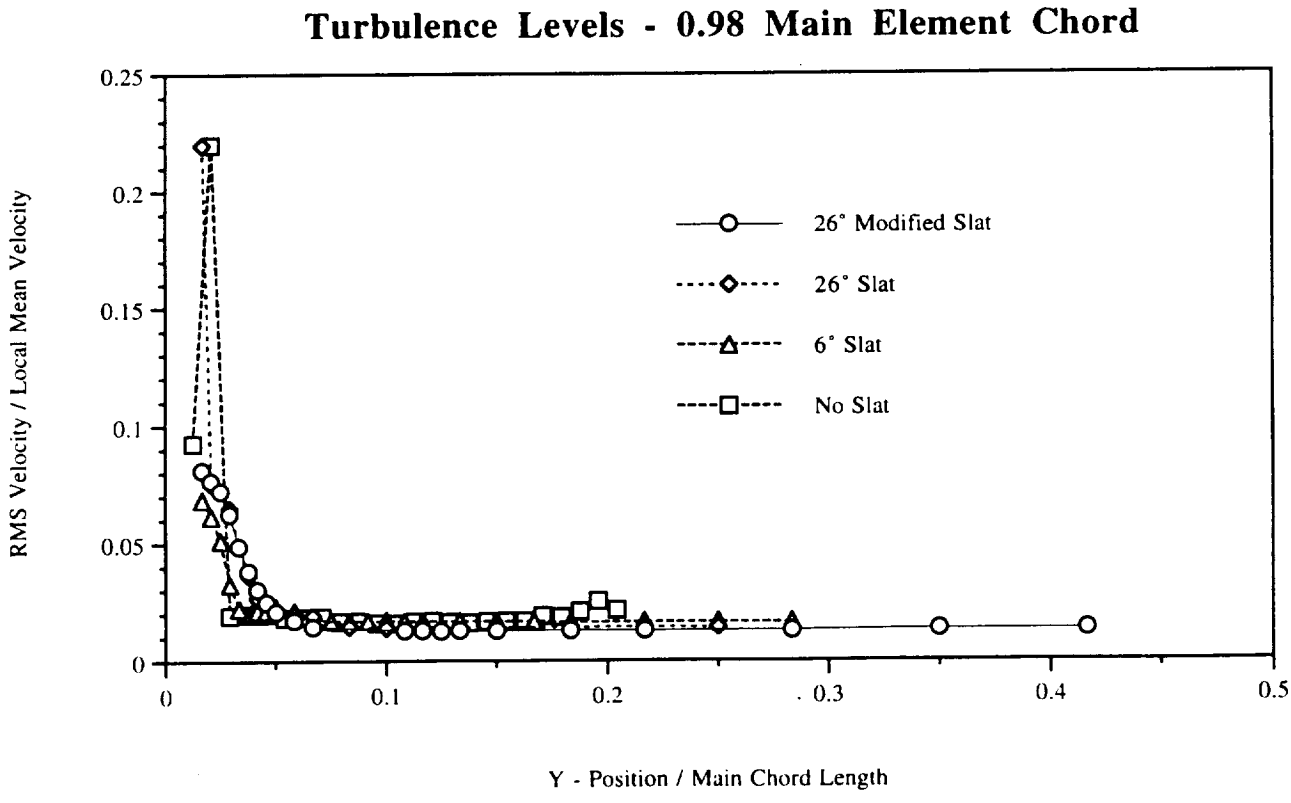
Turbulence Levels - 0.98 Main Element Chord
RMS Velocity / Local Mean Velocity
0.25
0.2
0.15
0.1
0.05
0
0
0.1
0.2
0.3
0.4
0.5
26° Modified Slat
26° Slat
6° Slat
No Slat
Y - Position / Main Chord Length

Figure 9

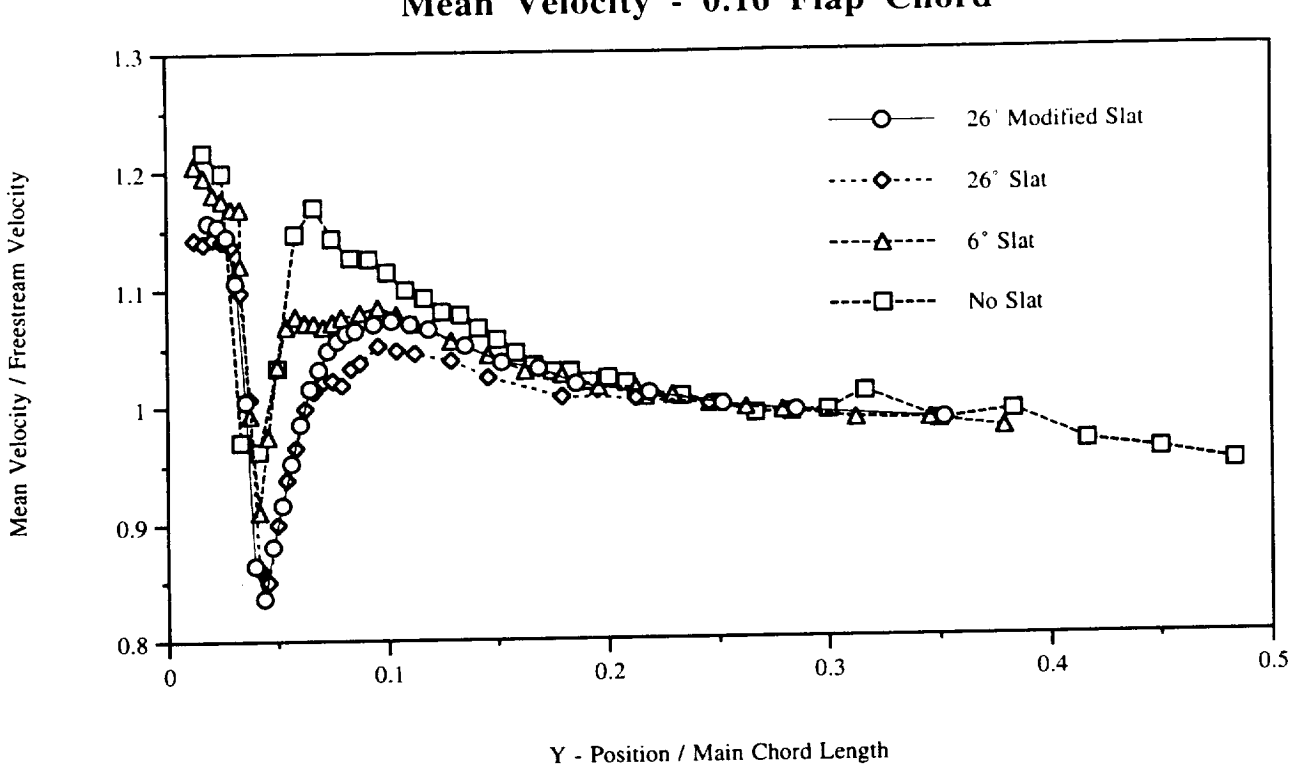
Mean Velocity - 0.16 Flap Chord
Mean Velocity / Freestream Velocity
1.3
1.2
1.1
1
0.9
0.8
0
0.1
0.2
0.3
0.4
0.5
26° Modified Slat
26° Slat
6° Slat
No Slat
Y - Position / Main Chord Length

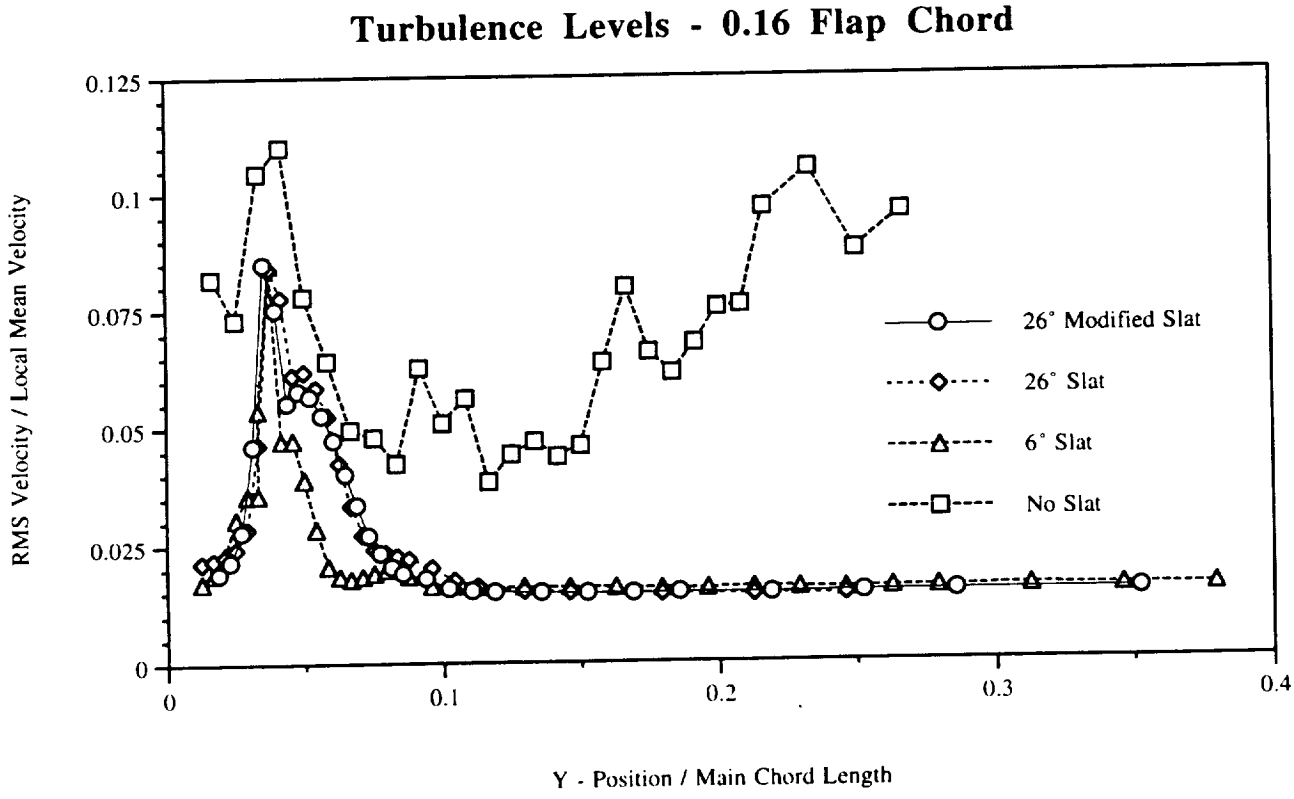
Turbulence Levels - 0.16 Flap Chord
RMS Velocity / Local Mean Velocity
0.125
0.1
0.075
0.05
0.025
0
0
0.1
0.2
0.3
0.4
26° Modified Slat
26° Slat
6° Slat
No Slat
Y - Position / Main Chord Length

Figure 10

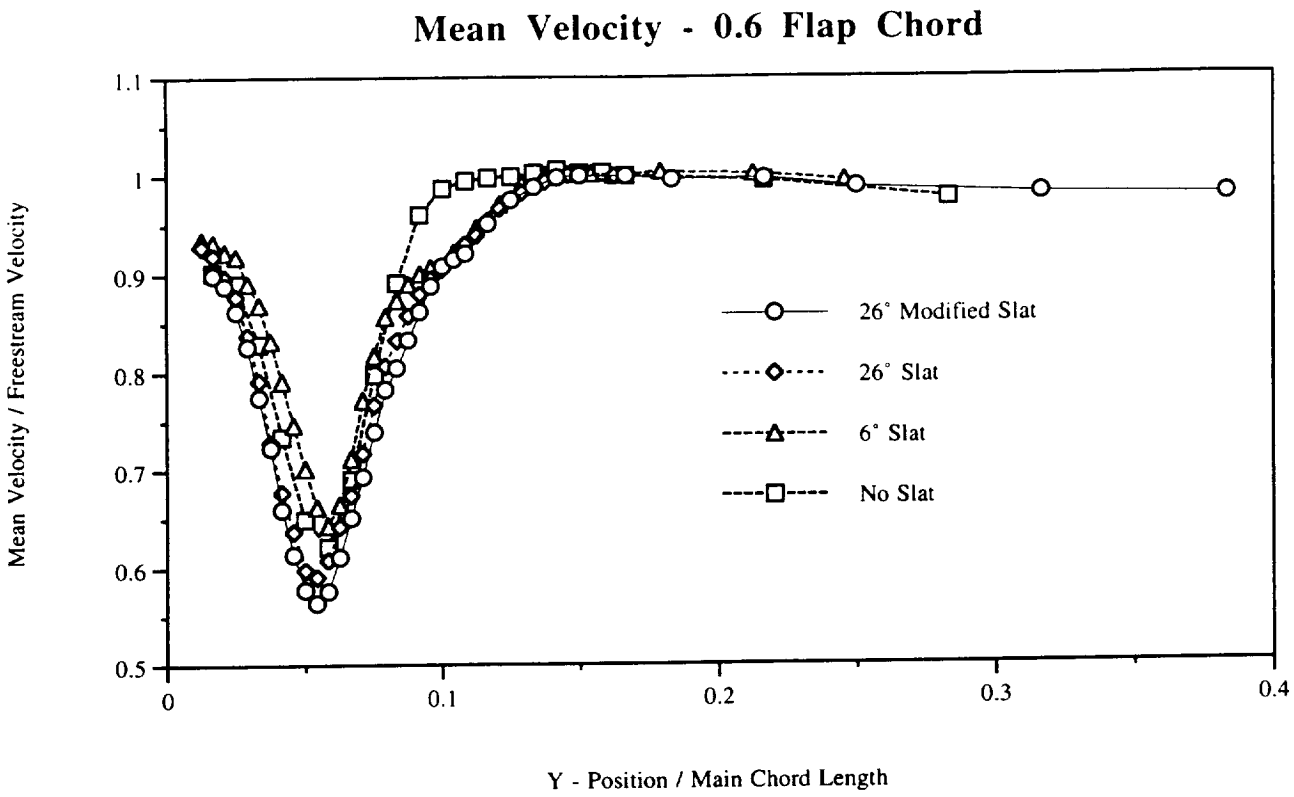
Mean Velocity - 0.6 Flap Chord
Mean Velocity / Freestream Velocity
1.1
1
0.9
0.8
0.7
0.6
0.5
0
0.1
0.2
0.3
0.4
26° Modified Slat
26° Slat
6° Slat
No Slat
Y - Position / Main Chord Length

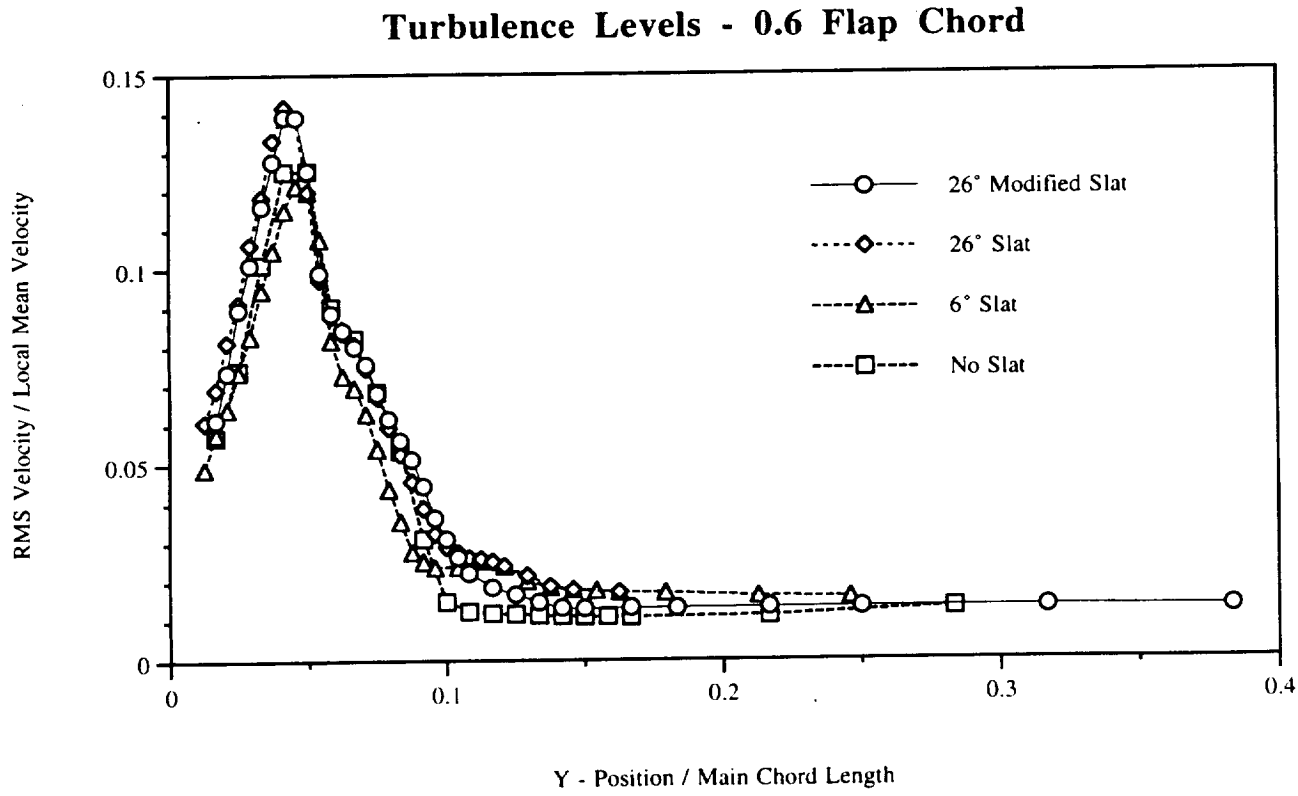
Turbulence Levels - 0.6 Flap Chord
RMS Velocity / Local Mean Velocity
0.15
0.1
0.05
0
0
0.1
0.2
0.3
0.4
26° Modified Slat
26° Slat
6° Slat
No Slat
Y - Position / Main Chord Length

Figure 11

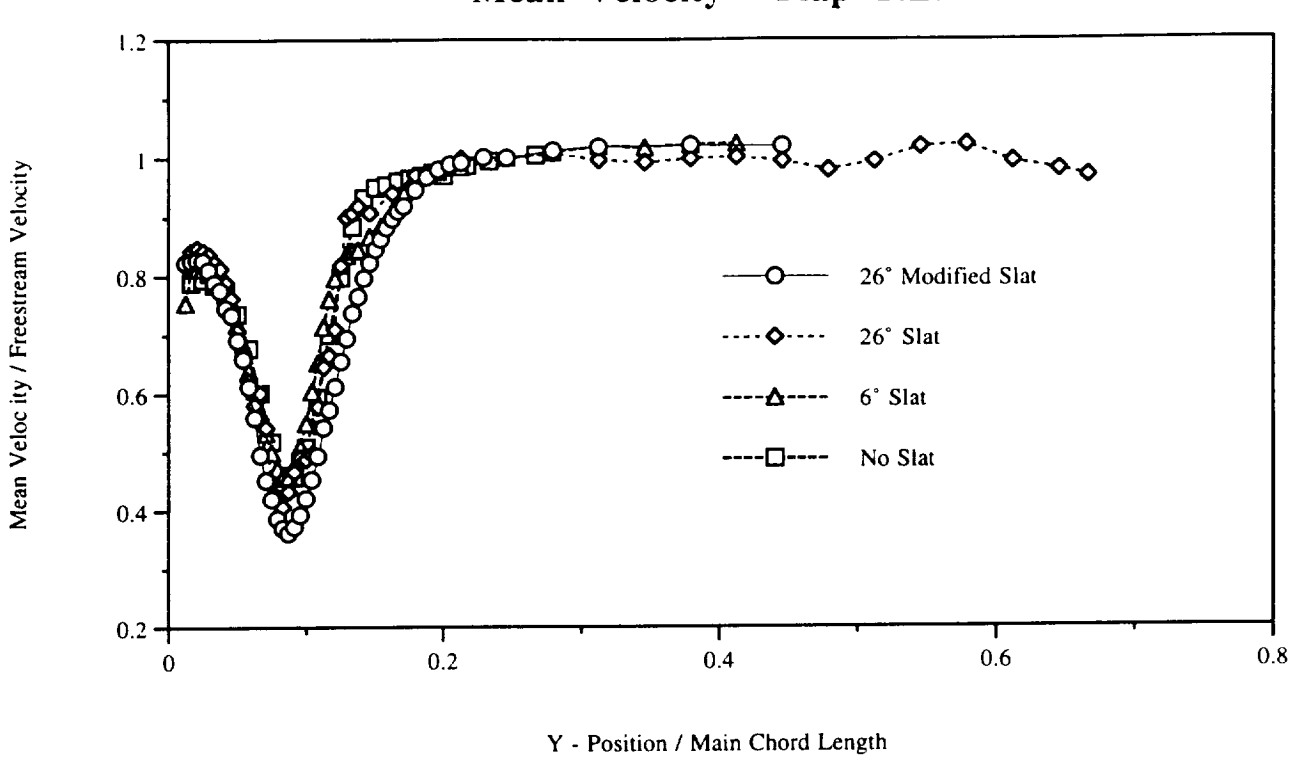
Mean Velocity - Flap T.E.
Mean Veloc ity / Freestream Velocity
1.2
1
0.8
0.6
0.4
0.2
0
0.2
0.4
0.6
0.8
26° Modified Slat
26° Slat
6° Slat
No Slat
Y - Position / Main Chord Length

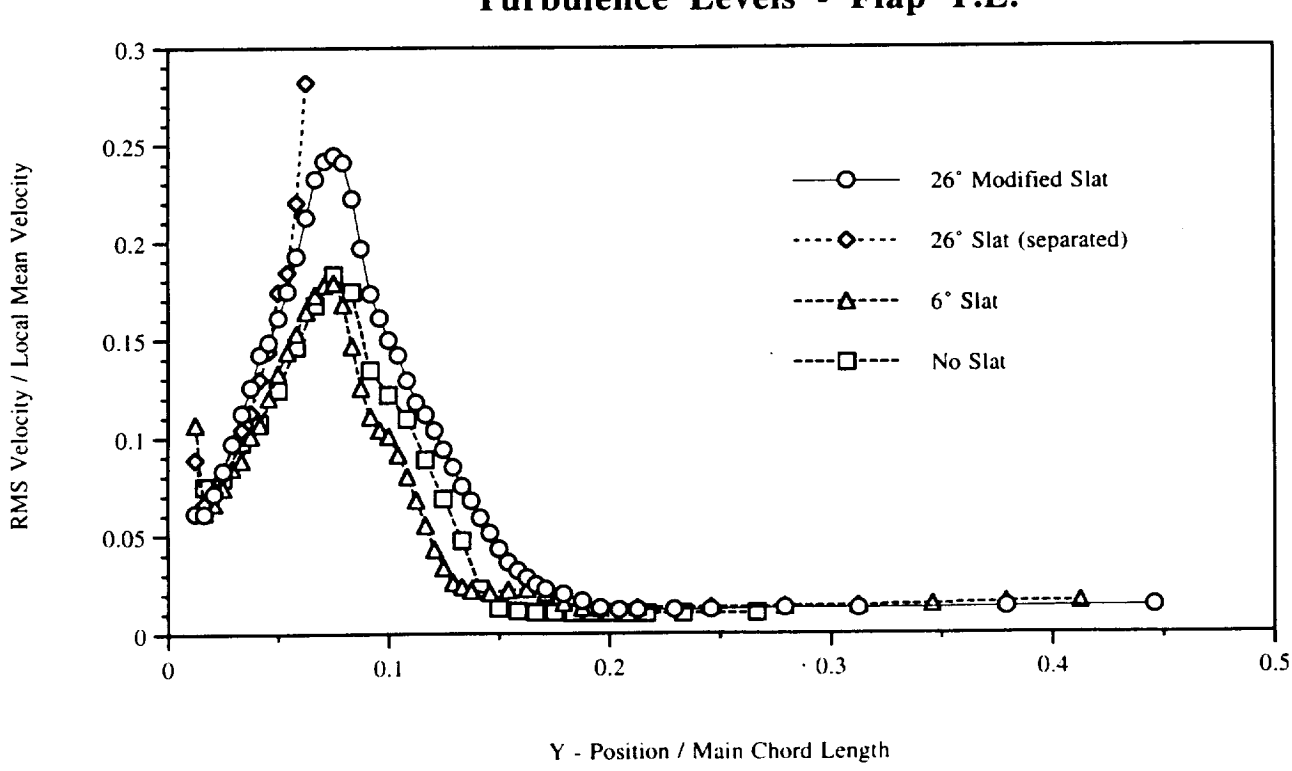
Turbulence Levels - Flap T.E.
RMS Velocity / Local Mean Velocity
0.3
0.25
0.2
0.15
0.1
0.05
0
0
0.1
0.2
0.3
0.4
0.5
26° Modified Slat
26° Slat (separated)
6° Slat
No Slat
Y - Position / Main Chord Length

Figure 12

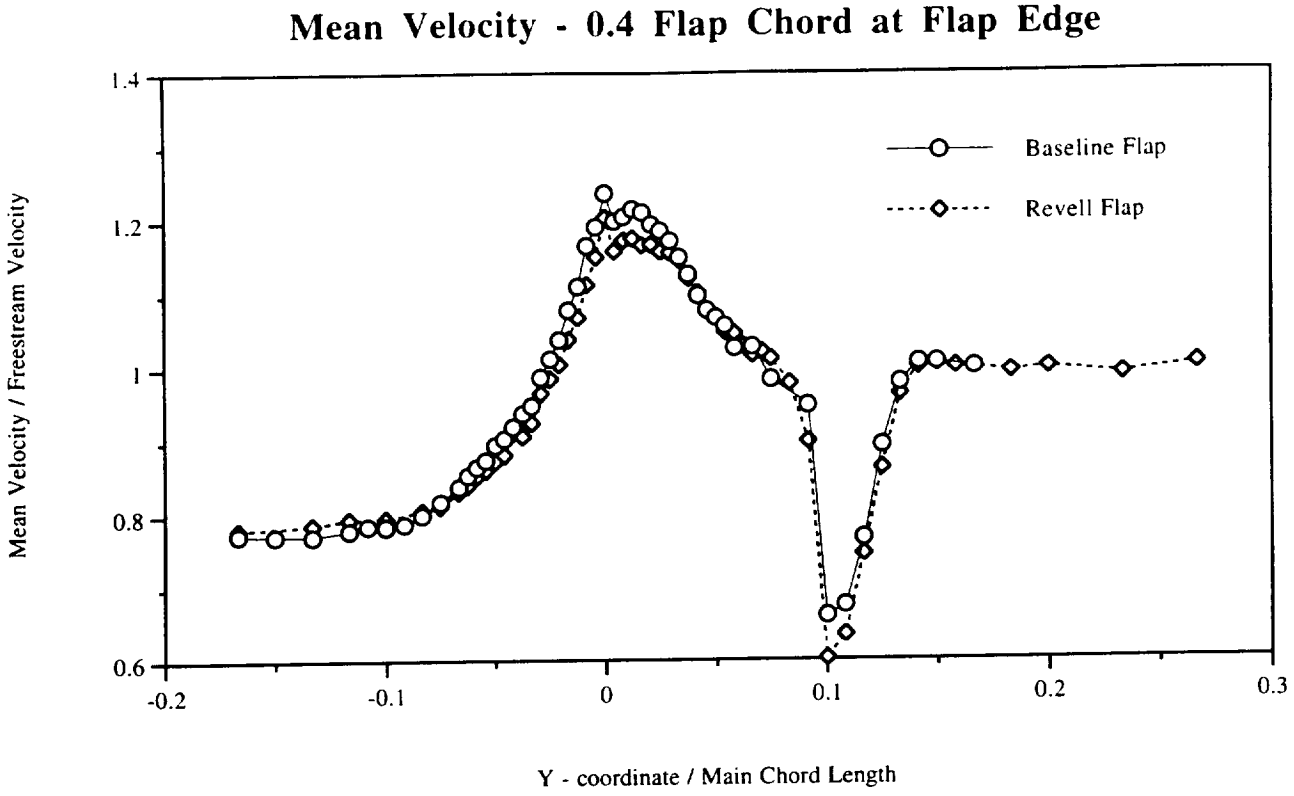
Mean Velocity - 0.4 Flap Chord at Flap Edge
Mean Velocity / Freestream Velocity
1.4
1.2
1
0.8
0.6
-0.2
-0.1
0
0.1
0.2
0.3
Baseline Flap
Revell Flap
Y - coordinate / Main Chord Length

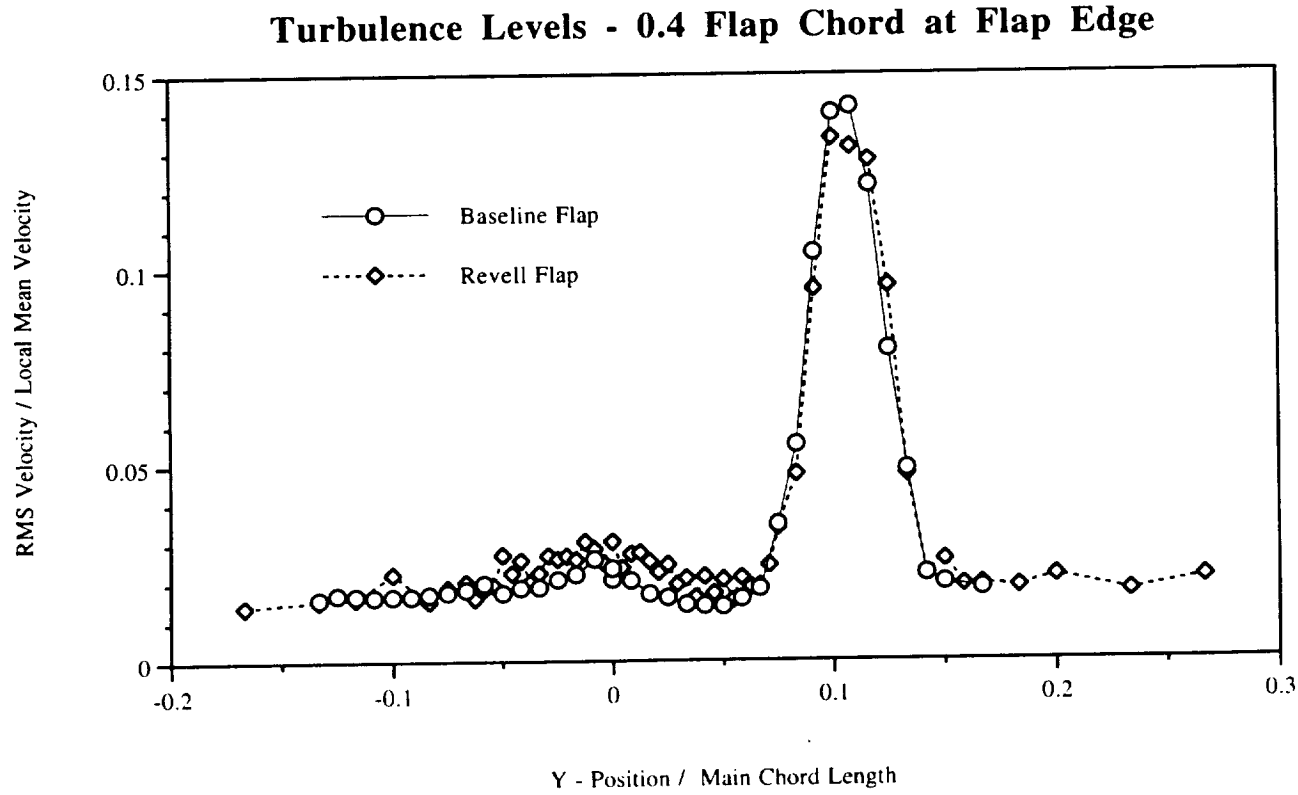
Turbulence Levels - 0.4 Flap Chord at Flap Edge
RMS Velocity / Local Mean Velocity
0.15
0.1
0.05
0
-0.2
-0.1
0
0.1
0.2
0.3
Baseline Flap
Revell Flap
Y - Position / Main Chord Length

Figure 13

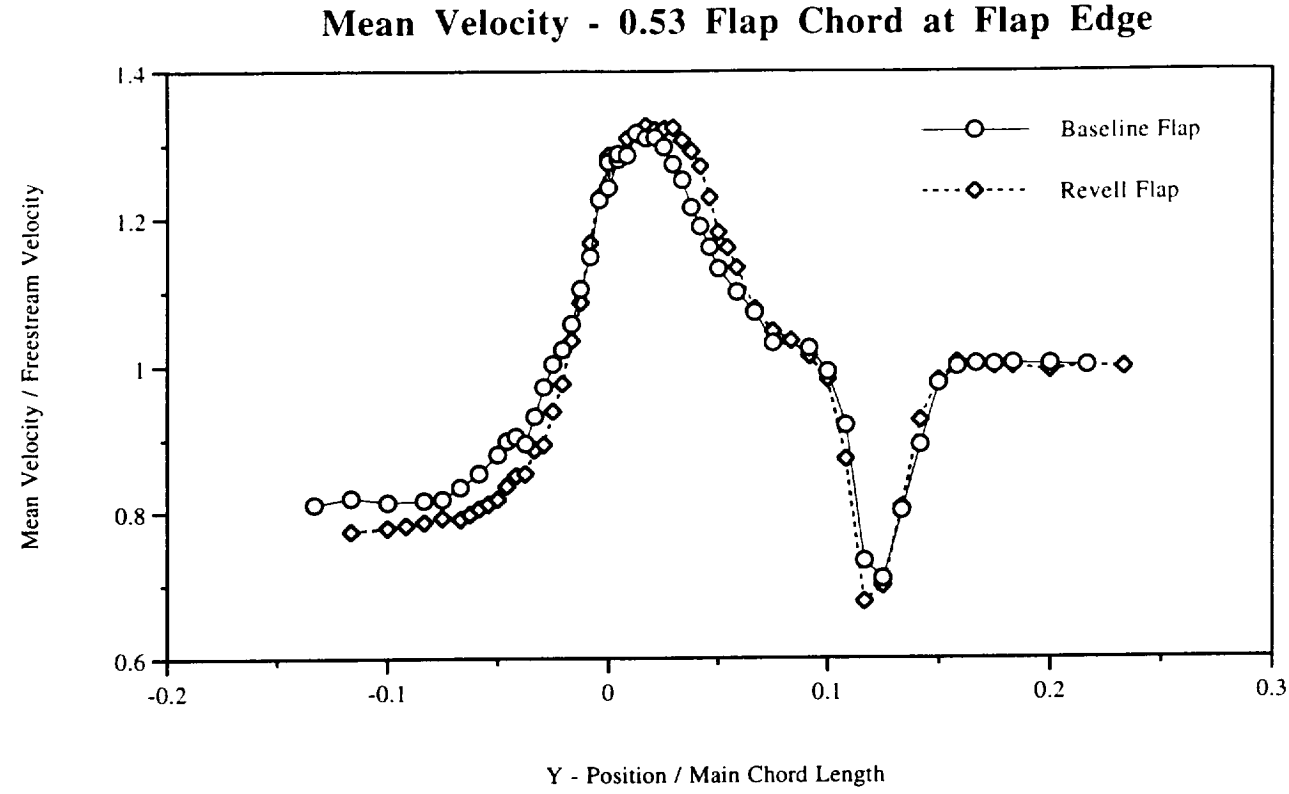
Mean Velocity - 0.53 Flap Chord at Flap Edge
Mean Velocity / Freestream Velocity
1.4
1.2
1
0.8
0.6
-0.2
-0.1
0
0.1
0.2
0.3
Baseline Flap
Revell Flap
Y - Position / Main Chord Length

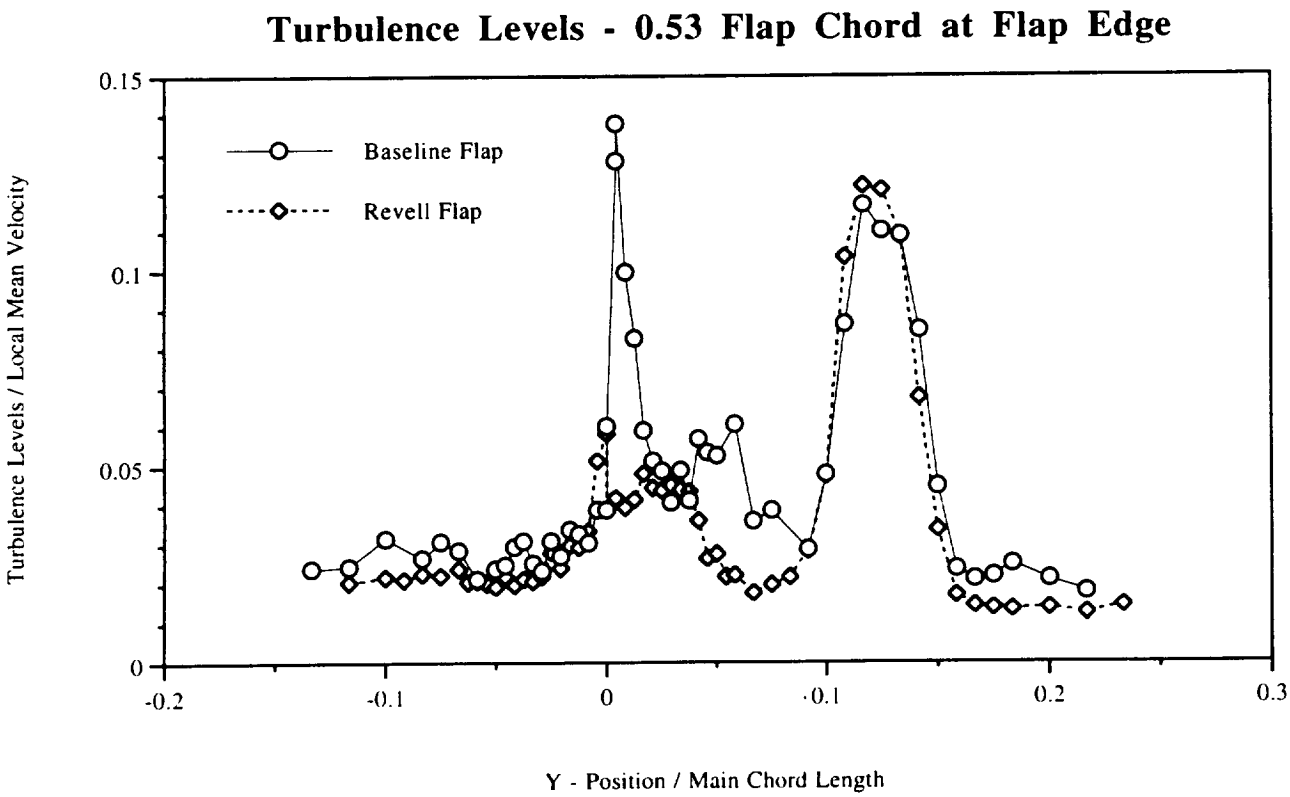
Turbulence Levels - 0.53 Flap Chord at Flap Edge
Turbulence Levels / Local Mean Velocity
0.15
0.1
0.05
0
-0.2
-0.1
0
0.1
0.2
0.3
Baseline Flap
Revell Flap
Y - Position / Main Chord Length

Figure 14

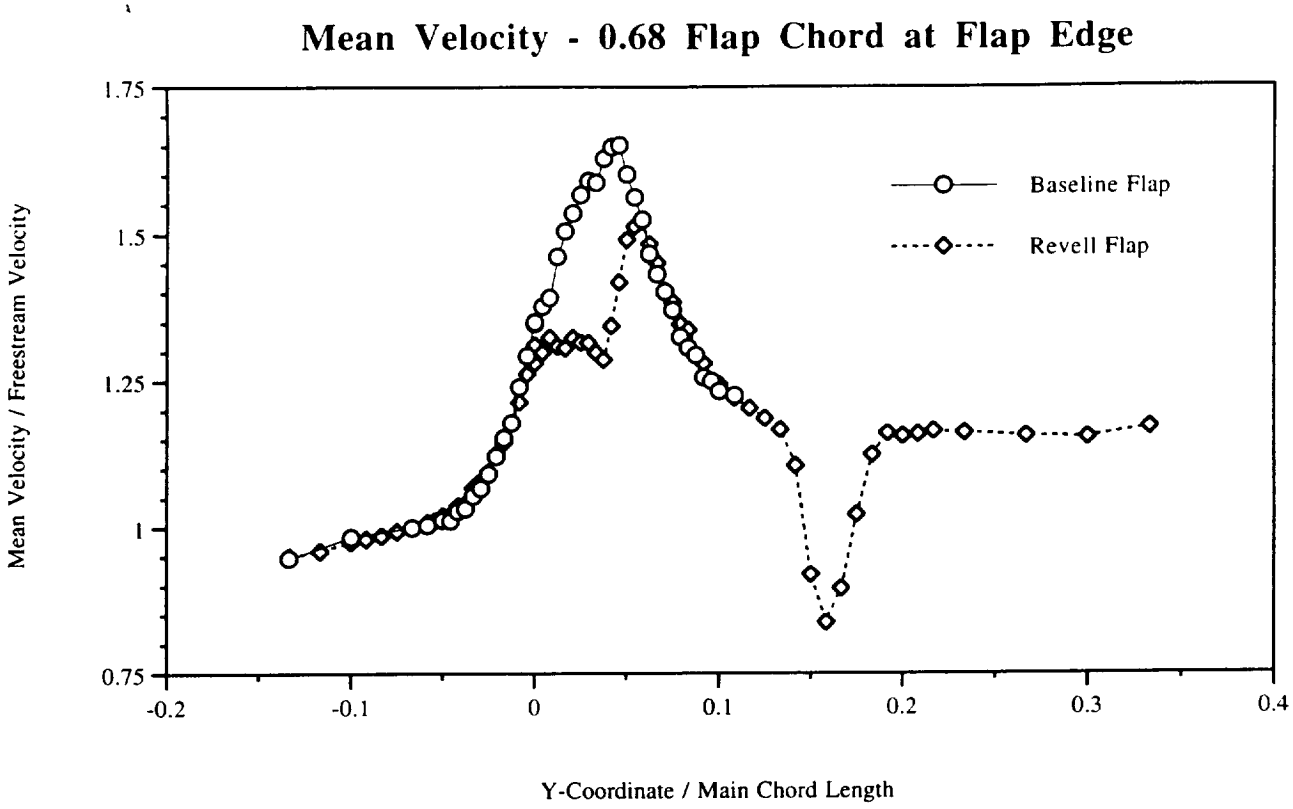
Mean Velocity - 0.68 Flap Chord at Flap Edge
Mean Velocity / Freestream Velocity
1.75
1.5
1.25
1
0.75
-0.2
-0.1
0
0.1
0.2
0.3
0.4
Baseline Flap
Revell Flap
Y-Coordinate / Main Chord Length

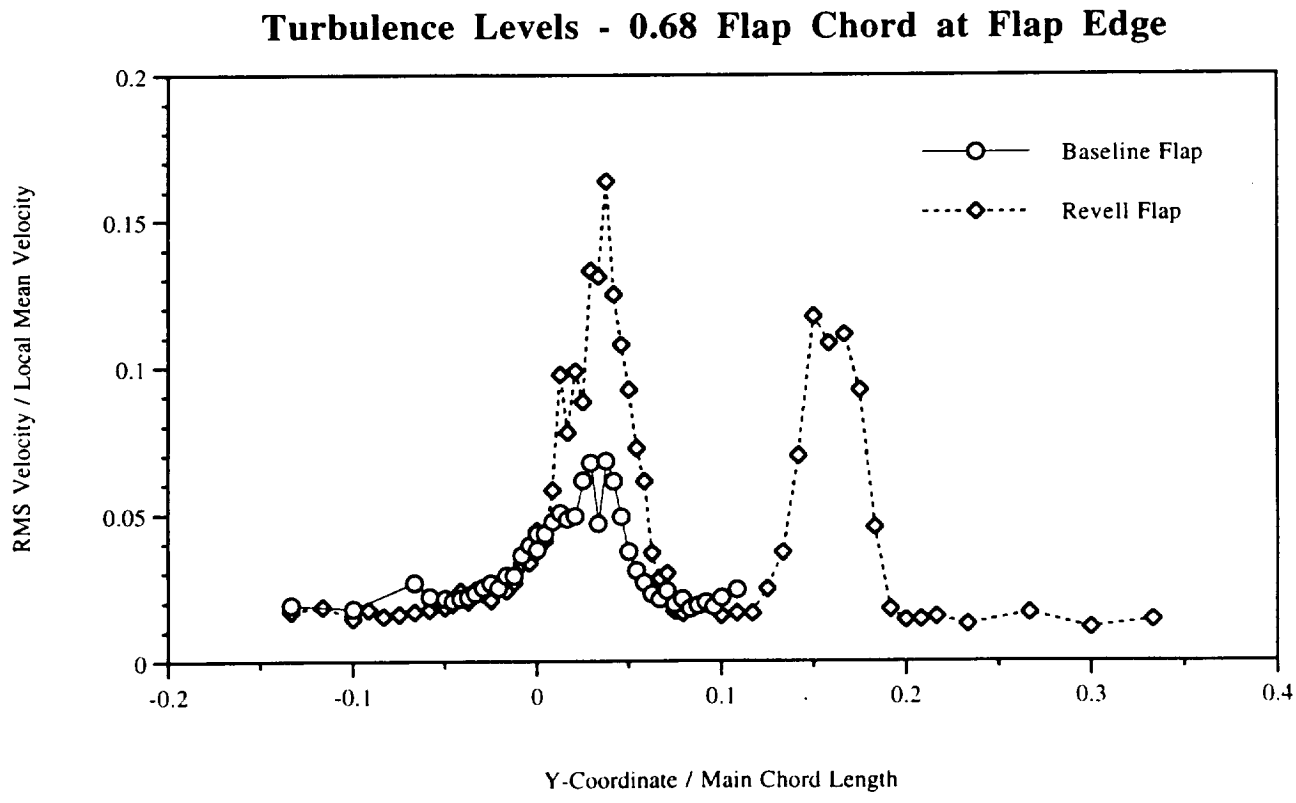
Turbulence Levels - 0.68 Flap Chord at Flap Edge
RMS Velocity / Local Mean Velocity
0.2
0.15
0.1
0.05
0
-0.2
-0.1
0
0.1
0.2
0.3
0.4
Baseline Flap
Revell Flap
Y-Coordinate / Main Chord Length

Figure 15

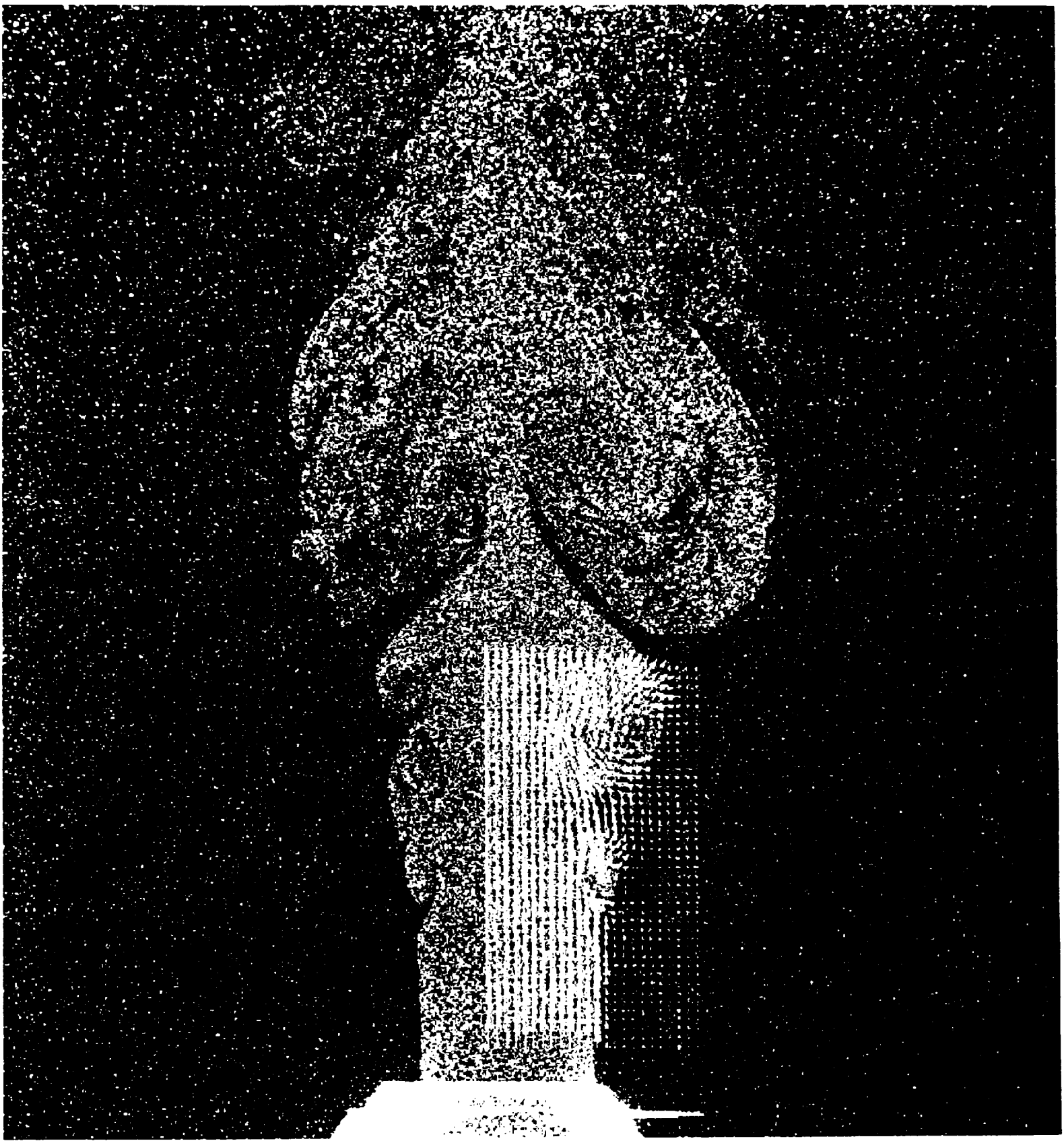

Figure 16. Sample Jet Image with Superimposed Velocity Vectors

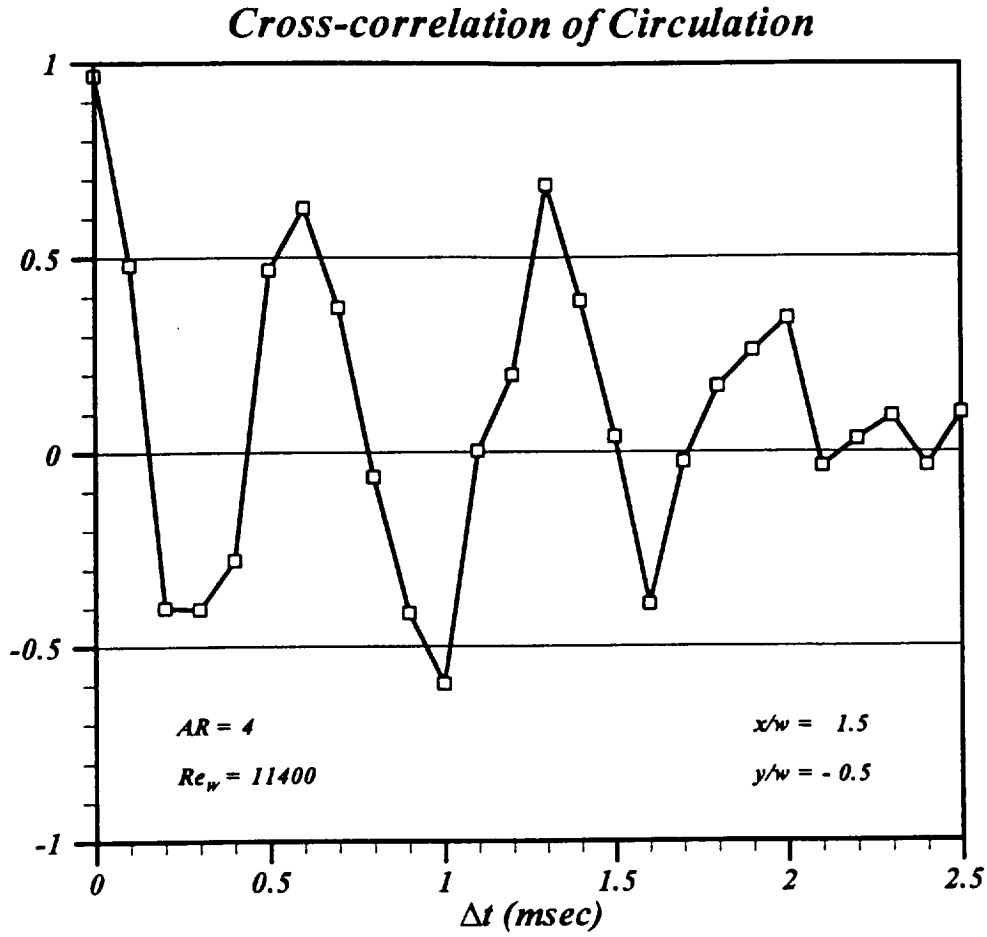
Cross-correlation of Circulation
1
0.5
0
-0.5
-1
0
0.5
1
1.5
2
2.5
Δt (msec)
AR = 4
Re_w = 11400
x/w = 1.5
y/w = - 0.5

Figure 17.

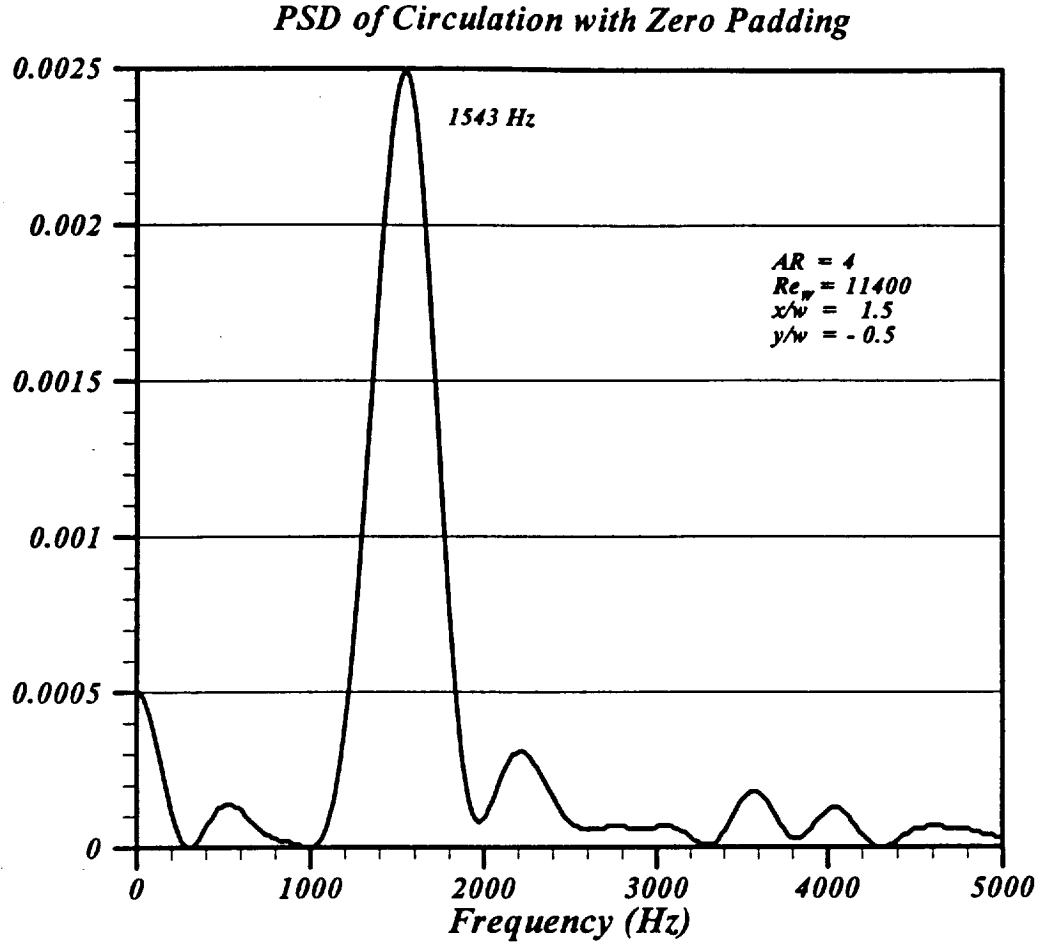
PSD of Circulation with Zero Padding
0.0025
0.002
0.0015
0.001
0.0005
0
1543 Hz
AR = 4
Re_w = 11400
x/w = 1.5
y/w = - 0.5
0
1000
2000
3000
4000
5000
Frequency (Hz)

Figure 18.

Appendix A : Experimental Setup for Cylinder and Flap Edge Tests

Cylinder Test Setup

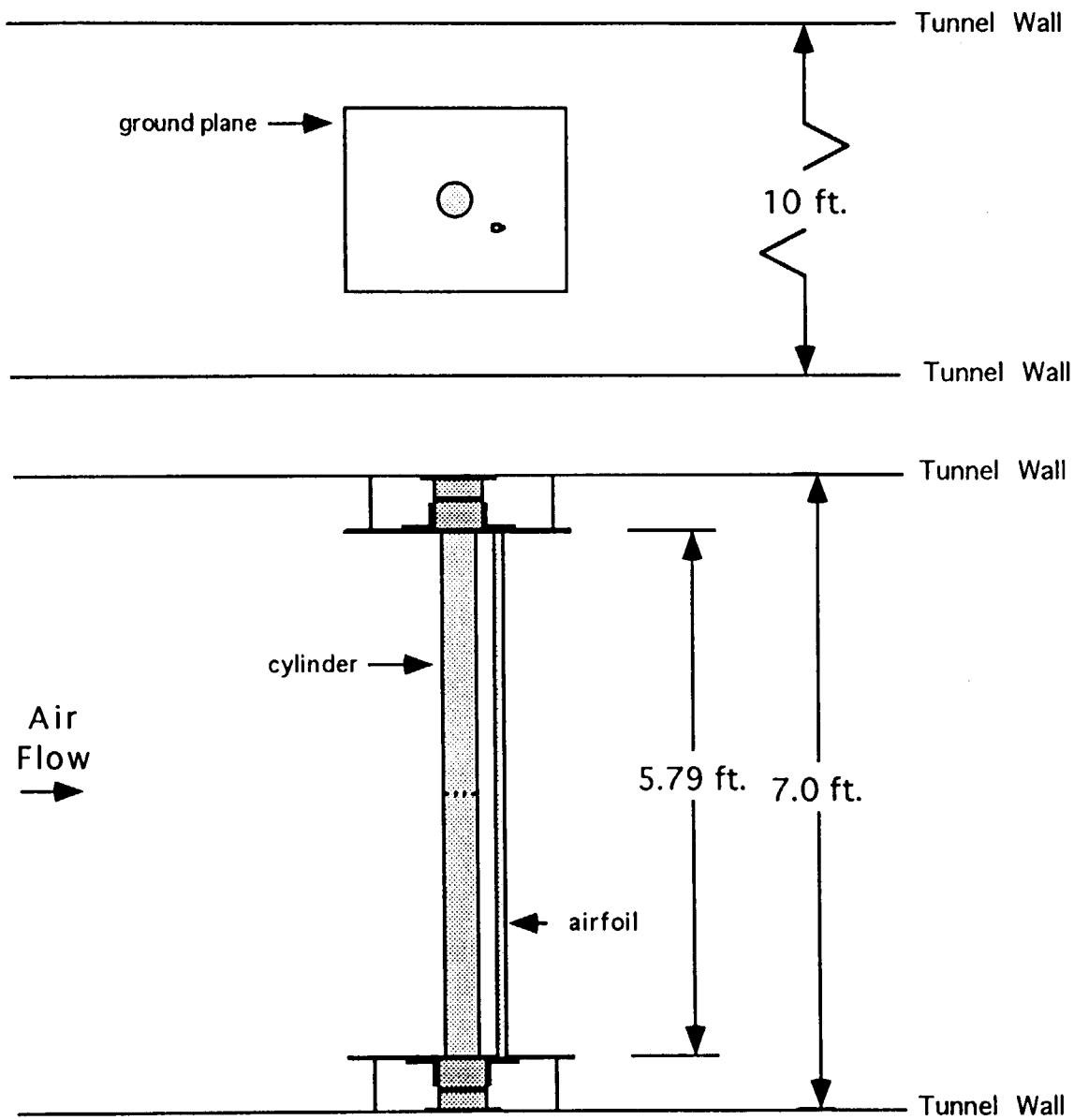

Position of Airfoil Section Relative to Cylinder

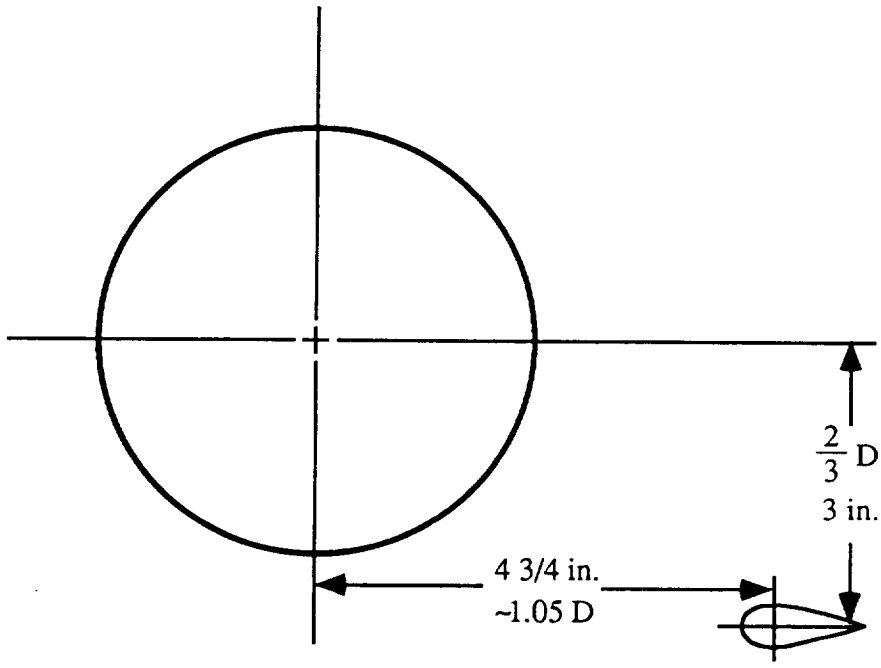

Wing Geometry with Hot-wire Measurement Planes

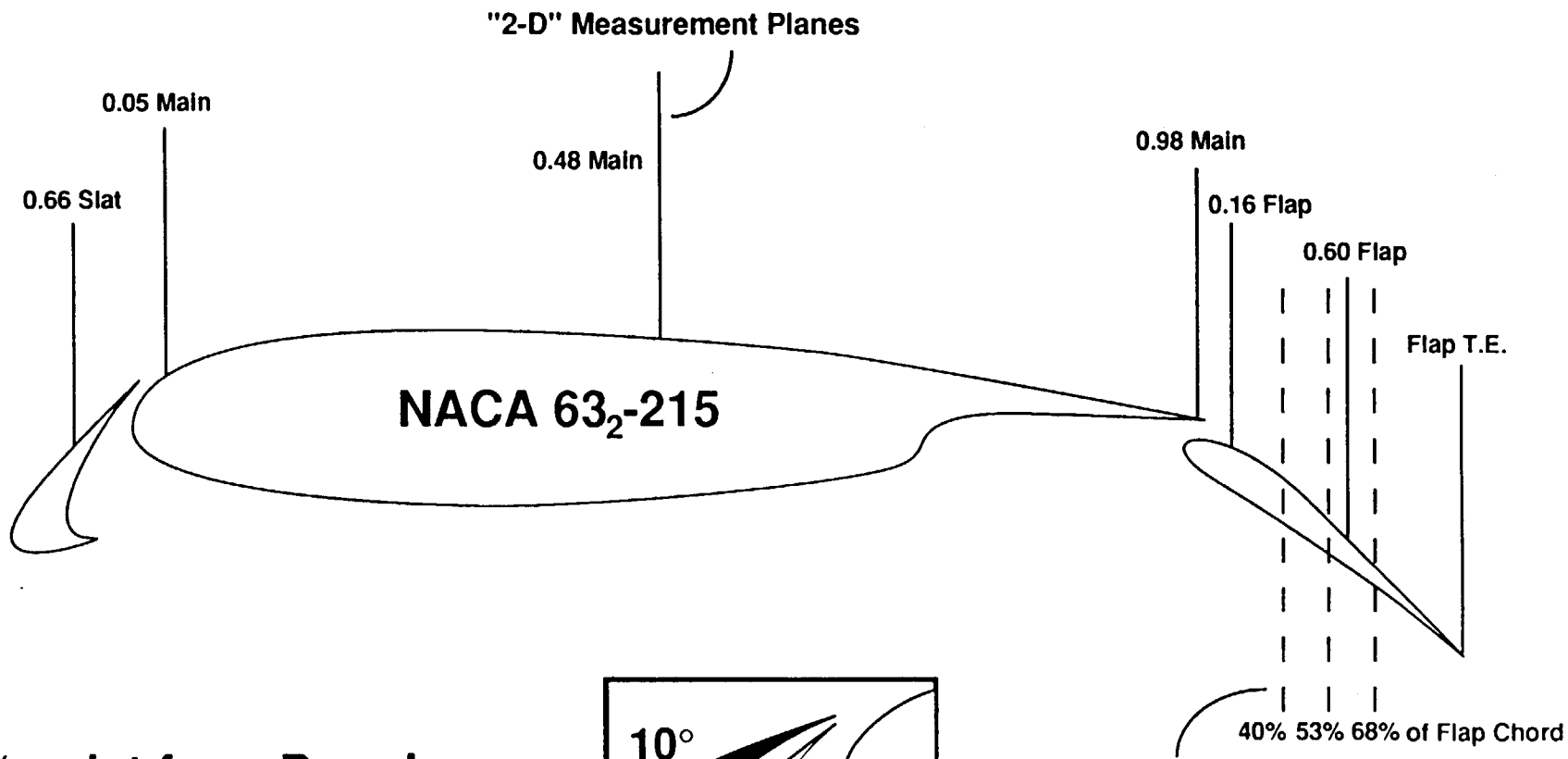

12%c slat from Douglas
3-element section (LB-546)

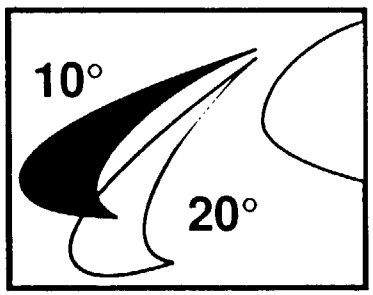

30%c Fowler flap

Top View of Wing with Hot-wire Measurement Planes

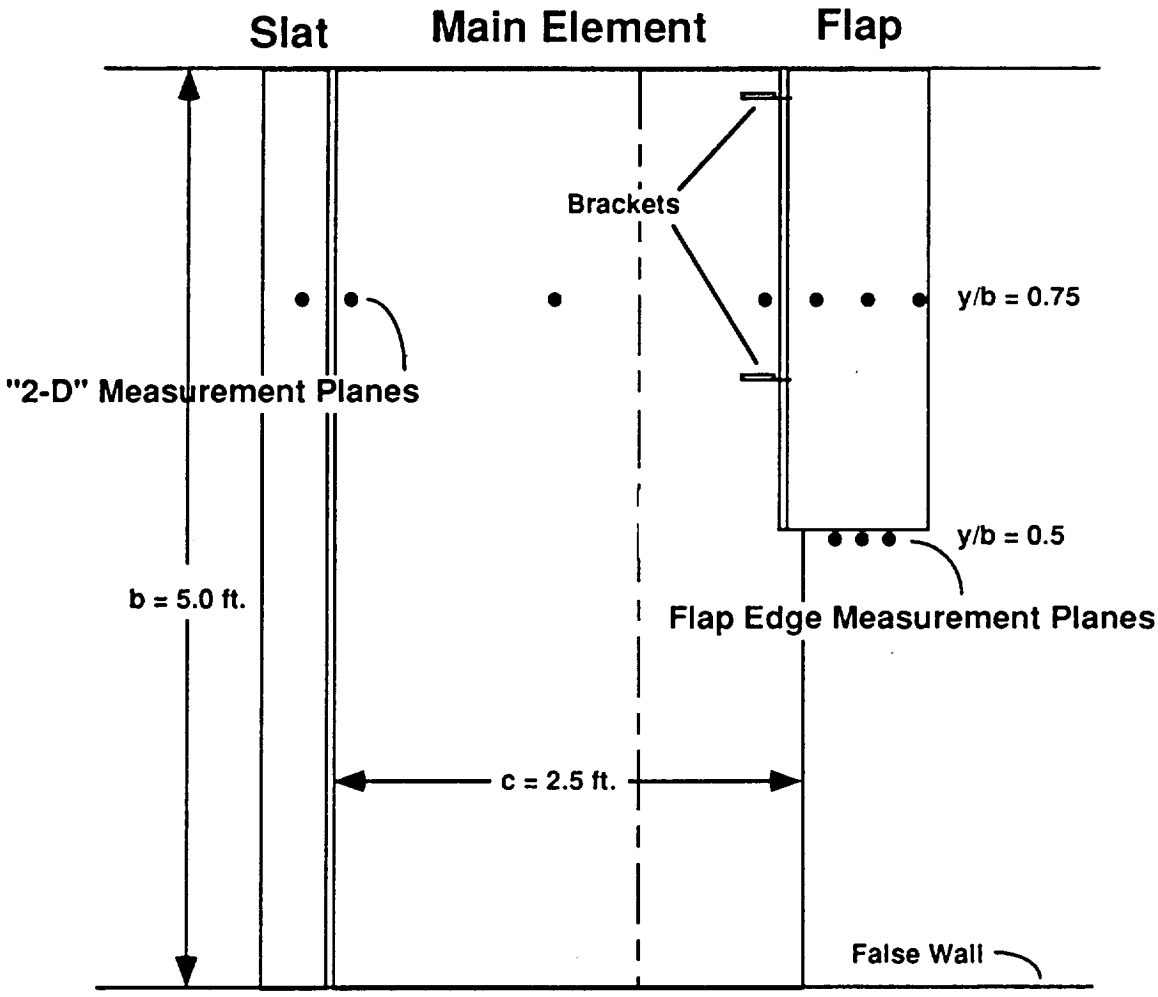

Appendix B: PIV Hardware

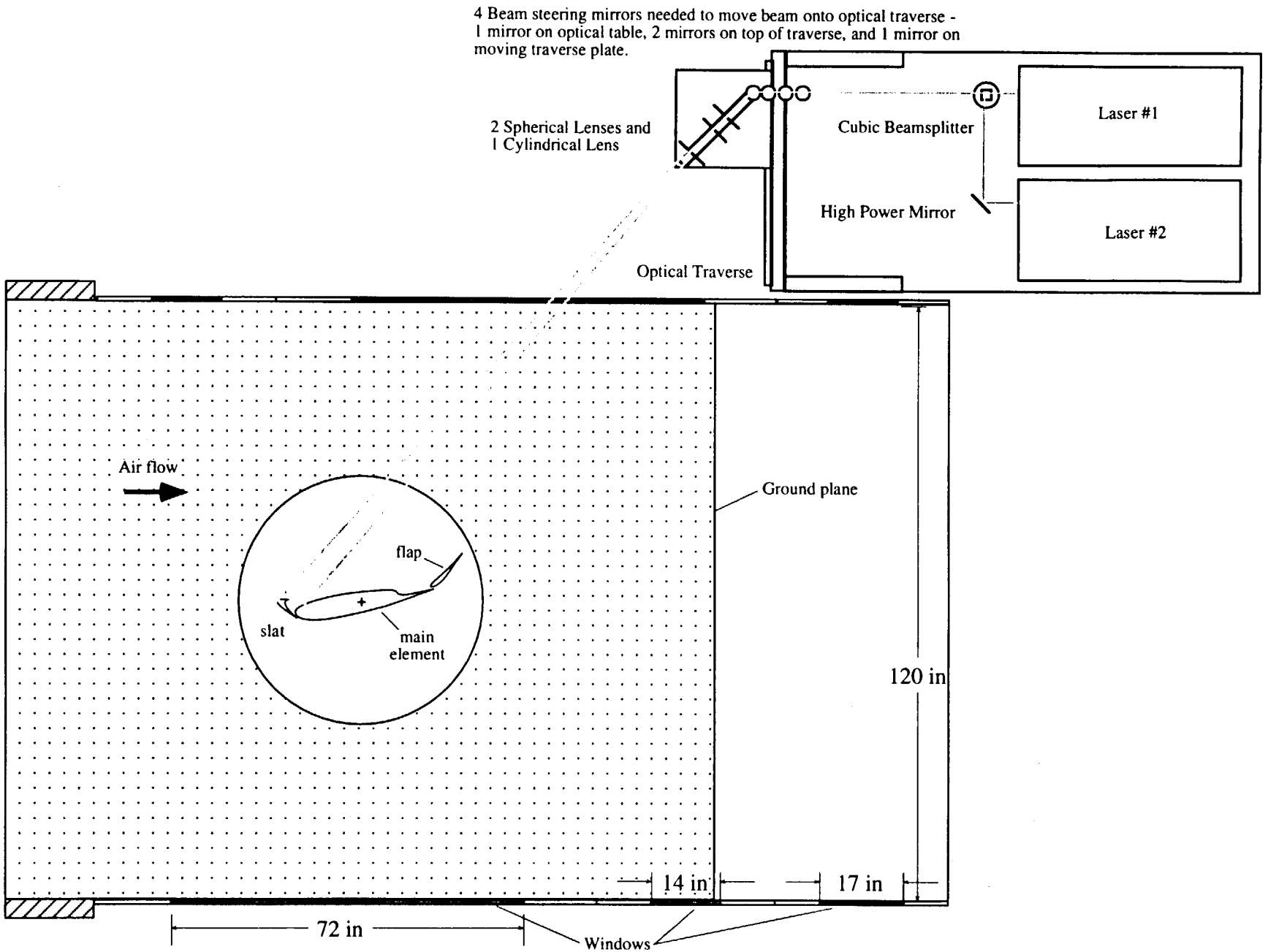
4 Beam steering mirrors needed to move beam onto optical traverse - 1 mirror on optical table, 2 mirrors on top of traverse, and 1 mirror on moving traverse plate.
2 Spherical Lenses and 1 Cylindrical Lens
Cubic Beamsplitter
Laser #1
High Power Mirror
Laser #2
Optical Traverse
Air flow
Ground plane
flap
slat
main element
120 in
14 in
17 in
72 in
Windows

Optical Traverse for Flap Edge III

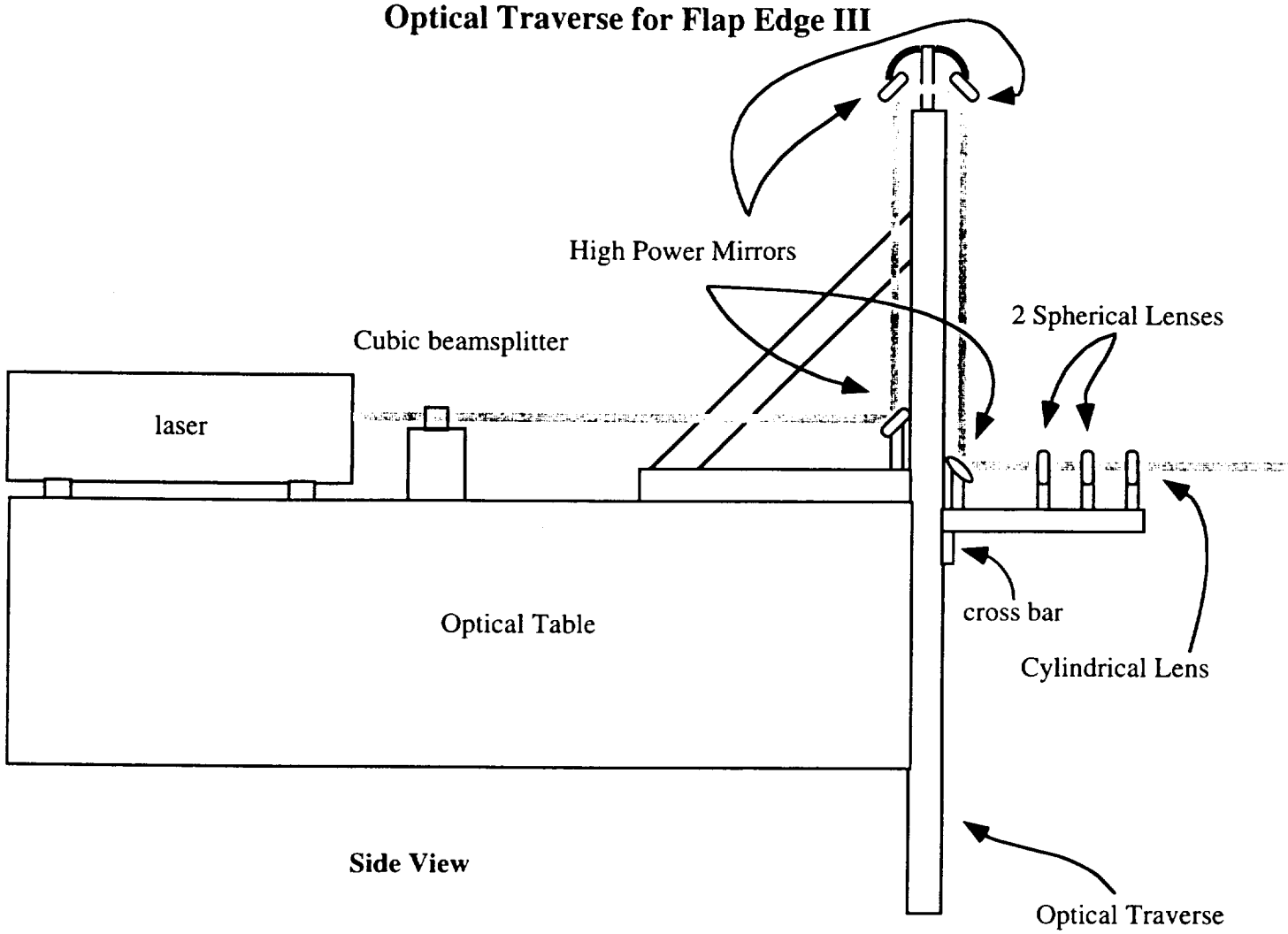

Side View

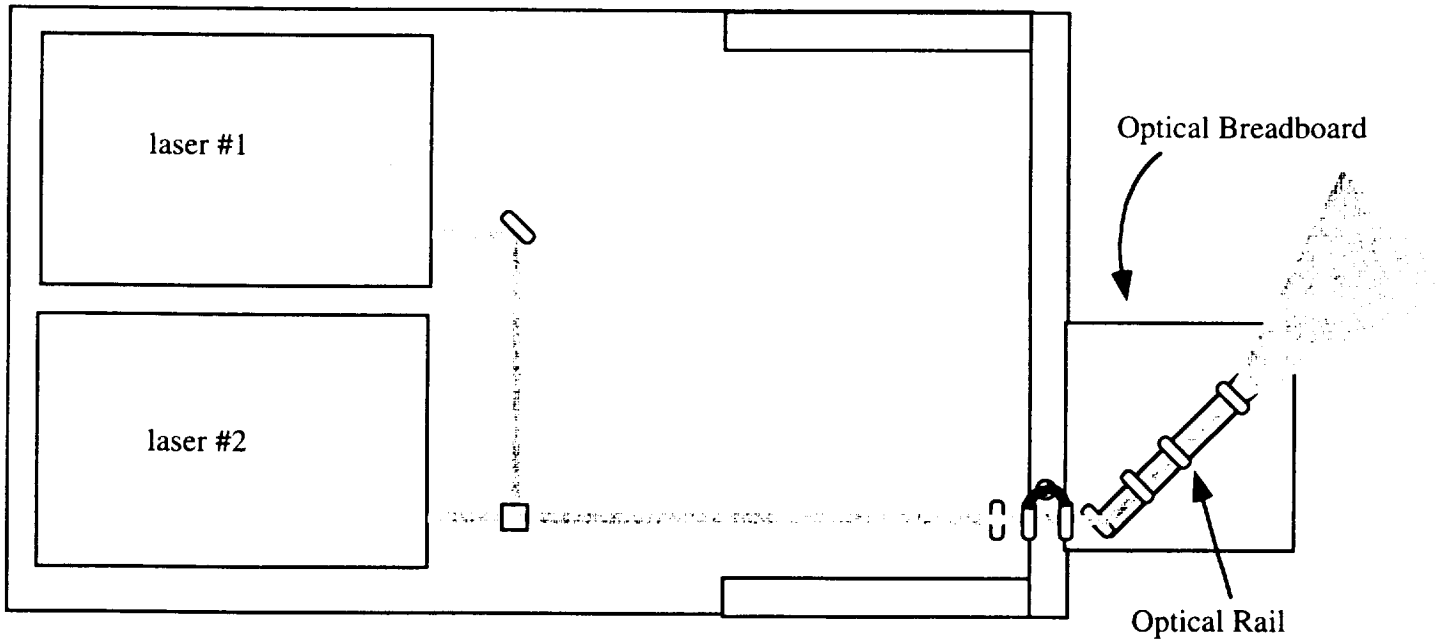

Top View

Camera Box

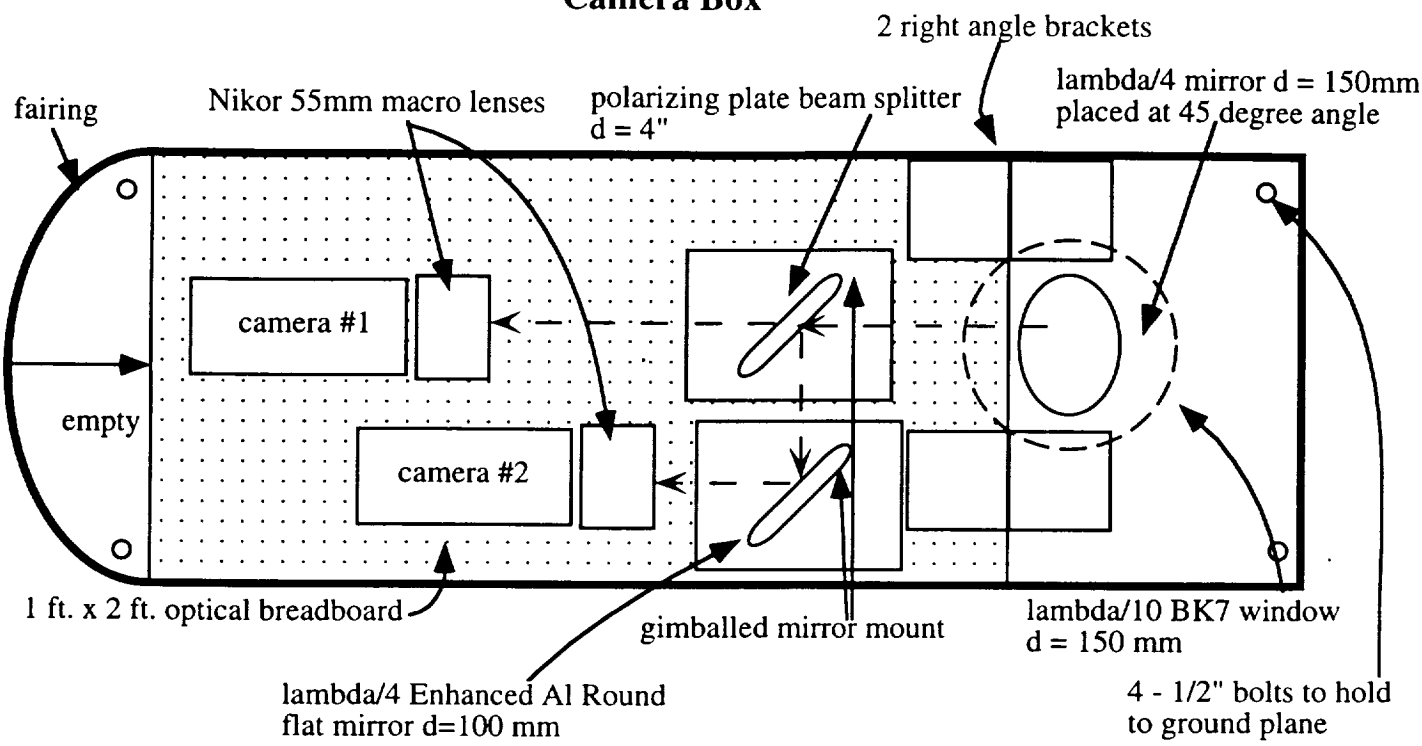
2 right angle brackets
fairing
Nikor 55mm macro lenses
polarizing plate beam splitter
d = 4"
lambda/4 mirror d = 150mm
placed at 45 degree angle
camera #1
empty
camera #2
1 ft. x 2 ft. optical breadboard
gimballed mirror mount
lambda/10 BK7 window
d = 150 mm
lambda/4 Enhanced Al Round
flat mirror d=100 mm
4 - 1/2" bolts to hold
to ground plane

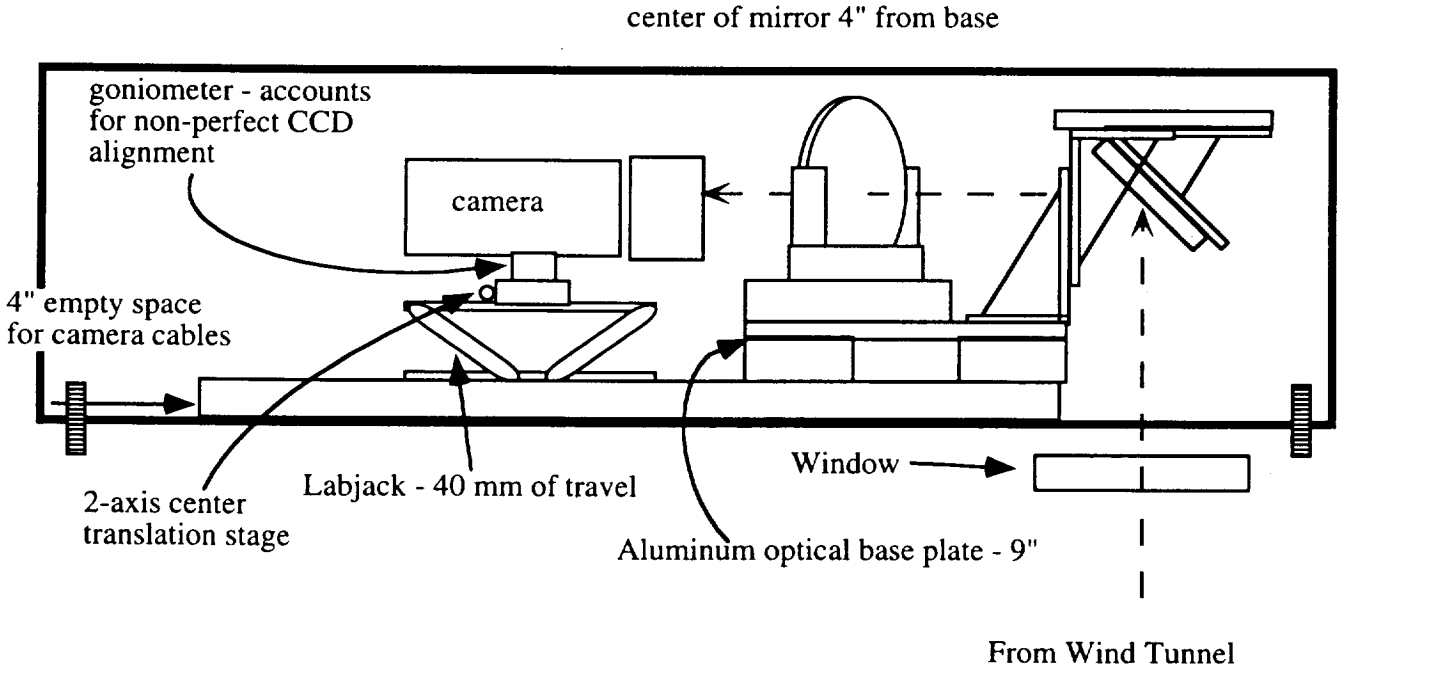
center of mirror 4" from base
goniometer - accounts
for non-perfect CCD
alignment
camera
4" empty space
for camera cables
2-axis center
translation stage
Labjack - 40 mm of travel
Window
Aluminum optical base plate - 9"
From Wind Tunnel

Ground Plane Window Placement

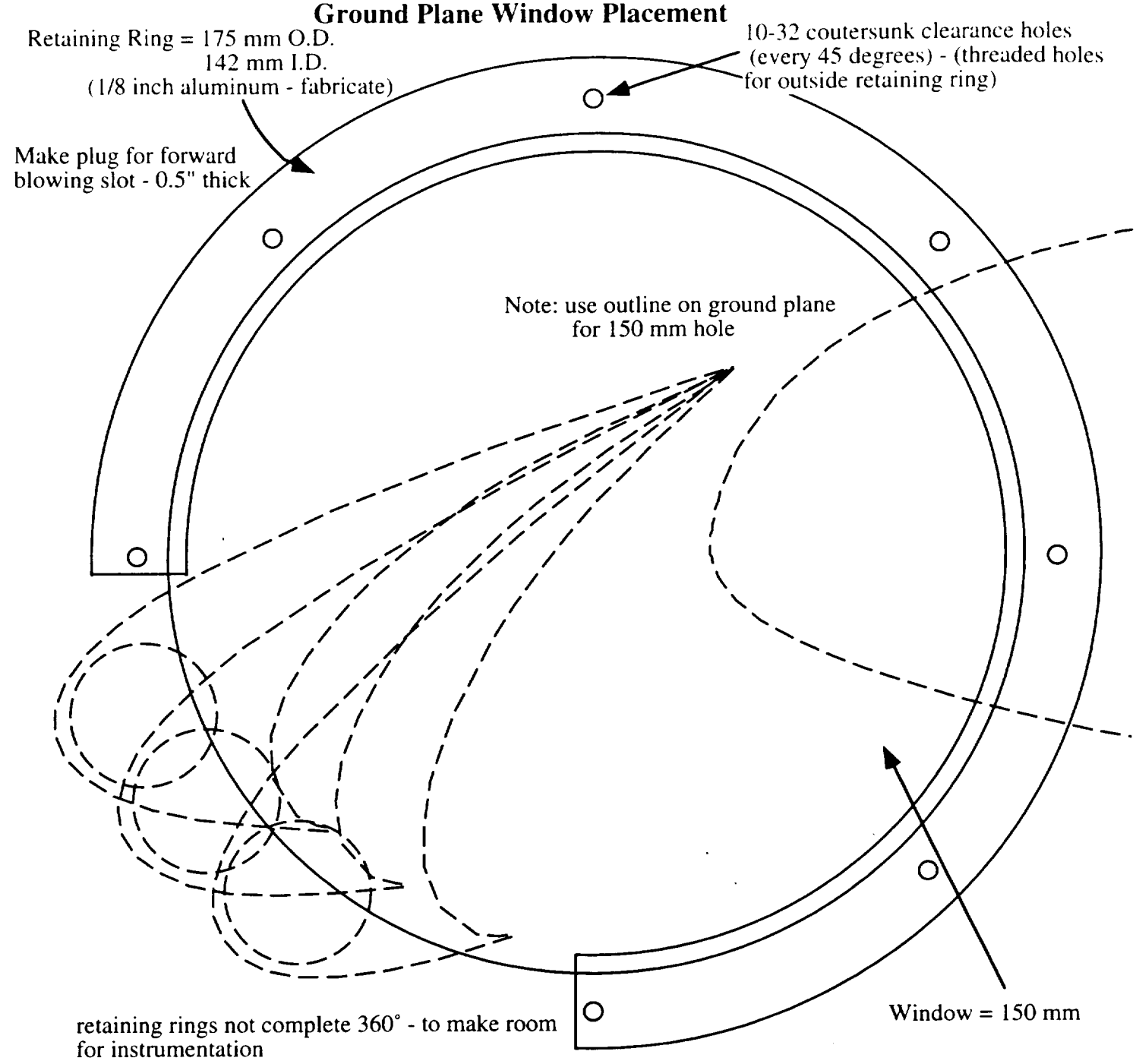

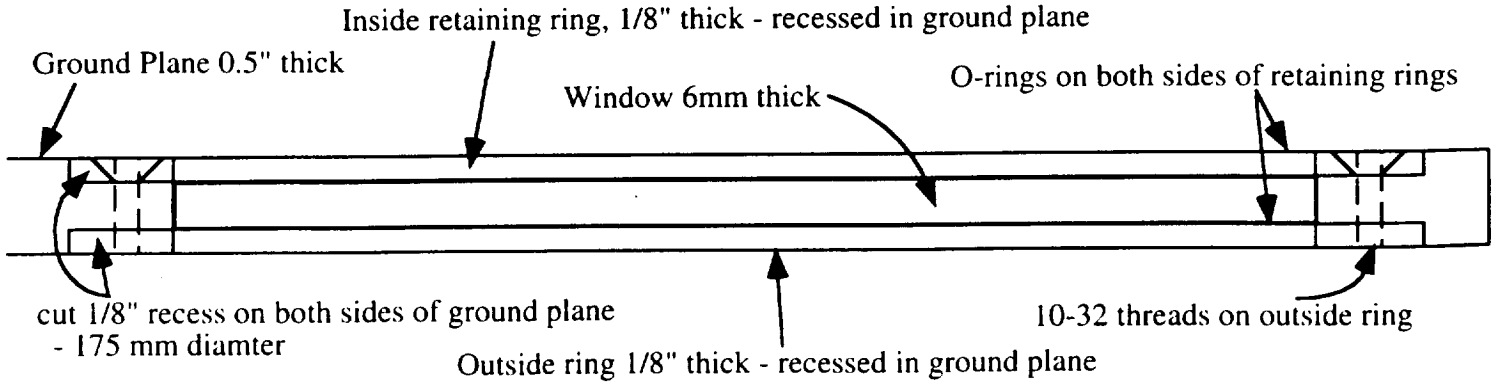

Make 150mm plug (6mm thick) and a 142 mm plug (1/8" thick) for when not using window (wood)